

1 **Introduction**

2 Tropospheric ozone (O₃) is a secondary air pollutant, i.e. it is not emitted as such in the air but
3 it is formed by reactions among precursors (e.g. CH₄, VOCs, NO_x). Ozone is an important
4 greenhouse gas resulting in a direct radiative forcing of 0.35-0.37 W m⁻² on climate (Shindell
5 et al., 2009; Ainsworth et al., 2012). Despite significant control efforts and legislation to
6 reduce O₃ precursor emissions, tropospheric O₃ pollution is still a major air quality issue over
7 large regions of the globe (Lefohn et al., 2010; Langner et al., 2012; Young et al., 2013;
8 Cooper et al., 2014; EEA, 2015; Sicard et al., 2016a,b; Ochoa-Hueso et al., 2017). Long-range
9 transport of O₃ and its precursors can elevate the local and regional O₃ background
10 concentrations (Ellingsen et al., 2008; Wilson et al., 2012; Paoletti et al., 2014; Derwent et al.,
11 2015; Xing et al., 2015; Sicard et al., 2016a). Therefore, remote areas such as the Arctic
12 region can be affected (Langner et al., 2012). The current surface O₃ levels (35-50 ppb in the
13 northern hemisphere, NH) are high enough to damage both forests and crops by reducing
14 growth rates and productivity (Wittig et al., 2009; Anav et al., 2011; Mills et al., 2011;
15 Ashworth et al., 2013; Proietti et al., 2016).

16

17 Increasing atmospheric CO₂, nitrogen deposition and temperatures enhance plant growth, and
18 increase primary production and greening of plants (Nemani et al., 2003; Zhu et al., 2016). At
19 the global scale, a widespread increase of greening and net primary production (NPP) is
20 observed over 25-50% of the vegetated area, while a decrease is observed over only 7% of the
21 globe (Nemani et al., 2003; Zhu et al., 2016). In contrast, a previous modeling study over
22 Europe shows how surface O₃ reduces the mean annual gross primary production (GPP) by
23 about 22% and the leaf area index by 15-20% (Anav et al., 2011). Similarly, Proietti et al.
24 (2016), using different *in-situ* measurements collected over 37 European forest sites, found a
25 GPP decrease (up to 30%) caused by O₃ during the time period 2000-2010. At global scale,
26 over the time period 1901-2100, GPP is projected to decrease by 14-23% (Sitch et al., 2007).
27 As a consequence of reduced photosynthetic assimilation, the total biomass of trees is
28 estimated to be decreased by 7% under the current ground-level O₃ mean concentrations (40
29 ppb on average) and by 17% at mean O₃ concentrations expected in 2100 (97 ppb based on a
30 meta-analysis) compared to preindustrial O₃ levels in NH (about 10 ppb, Wittig et al., 2009).
31 From experiments, Wittig et al. (2009) also reported that the total tree biomass of
32 angiosperms was reduced by 23% at O₃ mean concentrations of 74 ppb, and by 7% at 92 ppb
33 for gymnosperms. High surface O₃ levels, exceeding 40 ppb, do occur in many regions of the
34 globe with associated economic costs of several billion dollars per year (Wang and Mauzerall,

35 2004; Ashmore, 2005). Ashworth et al. (2013) reported an annual loss of 3.5% for wheat
36 (very O₃-sensitive) and 1.0% for maize (more O₃-tolerant) for Europe in 2010 relative to
37 2000, while Holland et al. (2006) estimated a €4.5 billion loss in the production of 23
38 common crop species, due to surface O₃ exposure by 2020 relative to 2000.

39

40 The international Tropospheric Ozone Assessment Report (TOAR) establishes a state-of-the-
41 art of global O₃ metrics for climate change, human health and crop/ecosystem research
42 (Lefohn et al., 2017). To assess the potential O₃ risk and protect vegetation from O₃, different
43 metrics are used: the European and US standard (AOT40 and W126, respectively) are based
44 on exposure-based metrics, while flux-based metrics have been introduced only recently
45 (UNECE, 2010; Klingberg et al., 2014; EEA, 2015). Unlike the exposure-based metrics,
46 which only rely on the surface O₃ concentration, the flux-based metrics were developed to
47 quantify the accumulation of damaging O₃ taken up by vegetation through the stomata over a
48 species-specific phenological time-window. These metrics also provide an information-rich
49 tool in assessing the relative effectiveness of air pollution control strategies in lowering
50 surface O₃ levels worldwide (Monks et al., 2015). By reducing plant photosynthesis and
51 growth, high surface O₃ levels will result in reduction in carbon storage by vegetation, and
52 finally an indirect radiative forcing as a consequence of the CO₂ rising in the atmosphere
53 (Sitch et al., 2007; Ainsworth et al., 2012). This rising CO₂ reduces stomatal conductance
54 which decreases O₃ flux into plants leading to increased O₃ levels in the air of 3-4 ppb during
55 the growing season over the NH by doubling of CO₂ concentration (Fiscus et al., 2005;
56 Sanderson et al., 2007).

57

58 Projected changes in ground-level O₃ vary considerably among models (Stevenson et al.,
59 2006; Wild, 2007) and emission scenarios. In earlier studies, the emissions of O₃ precursors
60 were based on a high population growth, leading to very high projected surface O₃
61 concentrations by 2100 (Stevenson et al., 2000; Zeng and Pyle, 2003; Shindell et al., 2006).
62 The last emission scenarios, i.e. the Representative Concentration Pathways (RCPs) were
63 developed as part of the Fifth Assessment Report of the Intergovernmental Panel on Climate
64 Change (Meinshausen et al., 2011; van Vuuren et al., 2011; Cubasch et al., 2013; Myhre et
65 al., 2013). These scenarios include e.g. different assumptions on climate, energy access
66 policies, and land cover and land use changes (Arneth et al., 2008; Kawase et al., 2011;
67 Kirtman et al., 2013). Until now, studies on O₃ pollution impacts on terrestrial ecosystems are
68 either limited to a single model or to particular regions (e.g. Clifton et al., 2014; Rieder et al.,

69 2015) and only a few applications of global or regional models under the new RCPs scenarios
70 were carried out (Kelly et al., 2012). In the framework of the Atmospheric Chemistry and
71 Climate Model Intercomparison Project (ACCMIP), different simulations were performed by
72 Lamarque et al. (2013) and Young et al. (2013) from 16 global chemistry models.

73

74 A few issues about surface O₃, such as a better understanding of spatial changes and a better
75 assessment of O₃ impacts worldwide, are still challenging. To overcome these issues, the aim
76 of this study is to quantify, for the first time, the spatial and temporal changes in the projected
77 potential O₃ impacts on photosynthetic carbon assimilation of vegetation at global scale, by
78 comparing the O₃ potential injury at present with that expected at the end of the 21st century
79 from different global chemistry models. The purpose of this study is not to provide a
80 quantitative estimation of the ecosystem injury due to O₃ but to highlight the world areas at
81 higher risk and changes by 2100.

82

83 **Materials and Methods**

84

85 *ACCMIP models and RCP scenarios*

86

87 The global chemistry models used in this work were developed under the ACCMIP project. A
88 detailed description of the selected models and of the emission scenarios (i.e. RCPs) is
89 included in Supplementary Information (SI). ACCMIP models were widely validated and
90 used to evaluate projected changes in atmospheric chemistry and air quality under different
91 emission and climate assumptions (e.g. Lamarque et al., 2010; Fiore et al., 2012; Bowman et
92 al., 2013; Lee et al., 2013; Voulgarakis et al., 2013). Lamarque et al. (2013) and Young et al.
93 (2013) provided the main characteristics of 16 models and details for the ACCMIP
94 simulations. Although within the ACCMIP project 16 models are available, due to the lack of
95 hourly O₃ concentration here we only focus on 6 global chemistry models with different
96 configurations (Table 1).

97

98 The length of historical and RCP simulations vary between models, but for all models the
99 historical runs cover a period centered around 2000, while the time-slice of RCPs is centered
100 around 2100 (Table 1). As for each model we compare the relative mean change between the
101 historical and RCP simulations, a different length in the number of years used in the analysis
102 does not affect the results.

103

104 ***Potential ozone injury on vegetation***

105

106 The O₃ exposure-based index, i.e. AOT40 (ppb h), is a metric used to assess the potential O₃
107 risk to vegetation from local to global scales (Emberson et al., 2014). In literature, AOT40 is
108 computed as sum of the hourly exceedances above 40 ppb, for hours between 8:00 hours and
109 20:00 hours or for hours with a solar radiation exceeding 50 Wm⁻² over species-specific
110 growing seasons (UNECE, 2010). Conventionally, two major growing-season time windows
111 are used, i.e. six months (April to September) for temperate climates, e.g. in Europe and all-
112 year round for Mediterranean, subtropical and tropical-type climates where vegetation is
113 physiologically active all along the year (Paoletti et al., 2007).

114

115 UNECE (2010) supports the use of a growing season, but a fixed time-window does not allow
116 incorporating the changes in the growing season due to climate change and would thus not be
117 well suited when investigating changes over time. A recent study over Europe showed how
118 computing AOT40 only over the growing season (i.e. April-September) would lead to an
119 underestimation of AOT40 up to 50% for conifer trees, while in case of deciduous trees the
120 underestimation is much smaller (< 5%, Anav et al., 2016). Besides, it should be noted that in
121 Anav et al. (2016) the AOT40 is computed year-round. We computed the AOT40 for a model
122 grid for hours between 8:00 hours and 20:00 hours (local time) for all days of the year.
123 Therefore, we computed AOT40 as follows:

124

125
$$\text{AOT40} = \int_{01\text{jan}}^{31\text{dec}} \int_{8\text{am}}^{8\text{pm}} \max([\text{O}_3] - 40, 0) dt \quad (1)$$

126

127 where [O₃] is hourly O₃ concentration (ppb) simulated by the models at the lower model layer
128 and *dt* is time step (1h). The function "maximum" ensures that only values exceeding 40 ppb
129 are taken into account. For the protection of forests, a critical level of 5 ppm.h calculated over
130 the growing season is recommended by UNECE (2010). Within the 2008/50/CE Directive,
131 the critical level for agricultural crops (3ppm.h) is adopted as the long-term objective value
132 for the protection of vegetation by 2020.

133

134 The use of a common fixed time-window (8-20h) all year-round at global level allows
135 skipping the use of a latitude model, which would increase the level of complexity and
136 uncertainties. Because the growing season is highly variable across the latitude, rather than
137 introducing further uncertainties by using a latitude model to simulate the growing season, we

138 applied here a simplified approach with a year-long growing season which should be
139 considered as a worst case study. This approach is valuable and can be easily applied at global
140 scale to compare the historical and projected potential risk to vegetation.

141
142 The O₃ concentration to be used in AOT40 calculation should be at the top of the canopy;
143 however, most of models used here provide O₃ concentrations at 90-120 m. Nevertheless,
144 even if the O₃ concentration is simulated at different elevations above the sea level, as for
145 each model we compare the variation between present and future, the change is consistent
146 because the elevation is the same. In case of risk assessment, by calculating AOT40 year-
147 round, an overestimation can be observed over polluted region of NH. Since the aim of this
148 study is to compare how O₃ stress to vegetation changes between historical period and future,
149 even if the AOT40 is misestimated at a given model grid point, as we compared the changes
150 in AOT40 at the same model grid point, the relative mean change is consistent.

151
152 From the AOT40, a factor of risk for forests and crops can be computed (Anav et al., 2011;
153 Proietti et al., 2016). Thus, the potential O₃ impact on photosynthetic carbon assimilation
154 (IO₃), in the worst-case scenario, is expressed through a dimensionless value as following:

$$155 \quad 156 \quad \text{IO}_3 = \alpha \times \text{AOT40} \quad (2)$$

157 where α is an empirically derived O₃ response coefficient representing the proportional
158 change in net photosynthesis per unit of AOT40 (Anav et al., 2011). From the Global Land
159 Cover Facility (GLCF) data at 1° of spatial resolution, we grouped the vegetation in three
160 categories: conifers, crops and deciduous trees. The relationships between cumulative ozone
161 exposure and reductions in net photosynthesis vary among and even within species (Reich,
162 1987; Ollinger et al., 1997). Differences in response per unit uptake tend to be greater in
163 magnitude between functional groups (e.g., hardwoods vs. conifers) where leaf structure and
164 plant growth strategy differ most widely (Reich, 1987). The dimensionless coefficient for
165 coniferous trees (0.7×10^{-6}) and crops (3.9×10^{-6}) are based on the regressions of the
166 photosynthesis response to O₃ (Reich, 1987), while the coefficient for deciduous trees
167 (2.6×10^{-6}) is based on Ollinger et al. (1997). From simulated changes in the risk factor, we
168 can highlight potential risk areas for vegetation.

170
171 **Results and Discussion**

172 Although differences in the simulated global O₃ spatial pattern were previously discussed and
173 analyzed (e.g. Lamarque et al., 2013), we show the mean annual O₃ concentration at the lower
174 model layer in Figure 1 because O₃ concentration explains AOT40 patterns. Then, in Figure 2
175 we show and discuss the AOT40 spatial and temporal distribution from the ACCMIP models
176 for the historical and RCPs simulations, and finally in Figure 3 we show the percentage of
177 variation of IO₃, i.e. the change in the potential impact of O₃ on photosynthetic carbon
178 assimilation for the ACCMIP models computed comparing the RCPs simulations with
179 historical runs. All spatial averages were calculated over land surfaces. A detailed description
180 of each figure, model by model, is included in Supplementary Information (SI).

181

182 **Spatial pattern of historical ozone concentration and AOT40**

183 The highest surface O₃ concentrations (Fig. 1) and potential O₃ impacts (Fig. 2) are found in
184 the NH, highlighting a hemispheric asymmetry. The multi-models O₃ mean concentration,
185 averaged over the land points of the domain, is 37.9 ± 4.3 ppb in NH and 22.9 ± 3.8 ppb in
186 SH (Table 3a). Over land surfaces, the NH extratropics (i.e. mid-latitudes beyond the tropics)
187 has 65% more O₃ than the SH extratropics (data not shown). Similarly, the highest AOT40
188 values are found in the NH, with an averaged AOT40 of 24.8 ± 10.1 ppm.h in NH and $2.5 \pm$
189 1.7 ppm.h in SH (Table 3a).

190

191 According to previous studies, the annual mean background O₃ concentrations at NH mid-
192 latitudes range between 35 and 50 ppb during the end of the 20th century (e.g. Cooper et al.,
193 2012; IPCC, 2014; Lefohn et al., 2014). Similarly, we found historical surface O₃ mean
194 concentrations ranging between 35 and 50 ppb and 35-50 ppm.h for AOT40 in the NH, with
195 the highest values occurring over Greenland and in the latitude band 15-45°N, particularly
196 around the Mediterranean basin, Near East, Northern America and over the Tibetan plateau (>
197 50 ppb and 70 ppm.h) while the lowest O₃ burden (15-30 ppb, < 20 ppm.h) was recorded in
198 SH, particularly over Amazon, African and Indonesian rainforests where the O₃ dry
199 deposition rate is maximum, up to 1.80 cm s^{-1} for mixed wood forests (Wesely and Hicks,
200 2000). Tropospheric O₃ has a significant source from stratospheric O₃ (Parrish et al., 2012)
201 and it can be transported by the large-scale Brewer-Dobson overturning circulation, i.e. an
202 upward motion from the tropics and downward at higher latitudes, resulting in higher O₃
203 concentrations in the extratropics (Hudson et al., 2006; Seidel et al., 2008; Parrish et al.,
204 2012). The six models are able to reproduce the spatial pattern of O₃ concentration and thus
205 AOT40 worldwide.

206

207 The highest historical O₃ mean concentrations are observed in GFDL-AM3 and the lowest are
208 found in MIROC-CHEM. In the early 2000s, the maximum global O₃ mean concentration (39
209 ppb) in GFDL-AM3 is associated to the lowest annual total NO_x emissions (46.2 Tg, Table
210 2a) and low LNO_x (4.4 Tg) while the minimum global O₃ mean concentration (28 ppb) in
211 MIROC-CHEM is related to the highest emissions of total NO_x per year (57.3 Tg) and
212 erroneously high LNO_x (9.7 Tg per year, Lamarque et al., 2013). MIROC-CHEM simulates
213 58 gaseous species in the chemical scheme with constant present-day biogenic VOCs
214 emissions while GFDL-AM3 simulates 81 species (Stevenson et al., 2012; Lamarque et al.,
215 2013). In GISS-E2-R, the hemispheric asymmetry in O₃ is more important with e.g. a mean
216 concentration of 22 ppb in SH and 42 ppb in NH. A stronger global AOT40 mean (26 ppm.h)
217 is observed in GISS-E2-R and the lowest (7 ppm.h) in MIROC-CHEM for historical
218 simulations. Model-to-model differences are observed due to different natural emissions of O₃
219 precursors (e.g. lightning NO_x) and the different chemical schemes used.

220

221 Higher O₃ burdens (mean concentration > 50 ppb, AOT40 >70 ppm.h) are simulated at high-
222 elevation areas, e.g. at Rocky and Appalachian Mountains and over the Tibetan plateau (Fig.
223 1, Fig. 2). At high-elevation, solar radiation, biogenic VOC emission, exchange between free
224 troposphere and boundary layer, and stratospheric O₃ intrusion within the troposphere are
225 more important than at the surface layer (Steinbacher et al., 2004; Kulkarni et al., 2011;
226 Lefohn et al., 2012). Altitude reduces the O₃ destruction by deposition and NO (Chevalier et
227 al., 2007). In addition, due to the high elevation, ambient air remains colder and dryer in
228 summer, leading to lower summertime O₃ losses from photolysis (Helmig et al., 2007). The
229 high-elevation areas, characterized by higher O₃ burdens, are well simulated in GISS-E2-R
230 and MOCAGE models.

231

232 The Tibetan plateau, so-called “ozone valley”, is the highest plateau in the world, with a mean
233 height of 4000 m a.s.l. (Tian et al., 2008) with strong thermal and dynamic influences on
234 regional and global climate (Chen et al., 2011). High surface O₃ mean concentrations (40-60
235 ppb) were reported in previous studies (e.g. Zhang et al., 2004; Bian et al., 2011; Guo et al.,
236 2015; Wang et al., 2015). Although this region is remote, road traffic, biofuel energy source,
237 coalmines and trash burning are prevalent. These pollution sources contribute to significant
238 amount of NO_x, CO and VOCs (Wang et al., 2015). The high O₃ levels are attributed to the
239 combined effects of high-elevation surface, thermal and dynamical forcing of the Tibetan

240 plateau and *in-situ* photochemical production in the air trapped in the plateau by surrounding
241 mountains (Guo et al., 2015; Wang et al., 2015). The dynamic effect, associated with the
242 large-scale circulation, is more important than the chemical effect (Tian et al., 2008; Liu et al.,
243 2010) and responsible for the high O₃ levels over the Tibetan plateau. The six models are able
244 to well reproduce the high surface O₃ mean concentrations (> 50 ppb) over the Tibetan
245 plateau.

246
247 Higher O₃ mean concentrations (> 60 ppb) are also observed in Southwestern U.S., at the
248 stations inland close to Los Angeles, in Northeastern U.S. and East Asia (e.g. Beijing) (Fig.
249 1). The American Southwest is an O₃ precursor hotspot where the industrial sources emit CH₄
250 and VOCs into the air (Jeričević et al., 2013) and the eastern and northern desert areas have
251 higher ambient O₃ than urban areas of southern California due to four factors: on-shore winds,
252 gasoline reformulation, eastward population expansion and nighttime air chemistry (Arbaugh
253 and Bytnerowicz, 2003). The surface concentrations show higher O₃ levels in areas downwind
254 of O₃ precursor sources, i.e. urban and well-industrialized areas, at distances of hundreds or
255 even thousands of kilometers due to transport of O₃ and precursors, including “reservoir”
256 species such as PAN, lower O₃ titration by NO and higher biogenic VOC emission (Wilson et
257 al., 2012; Paoletti et al., 2014; Monks et al., 2015; Sicard et al., 2016a). The higher O₃ levels
258 in areas downwind of O₃ precursor sources are well simulated in GISS-E2-R and MOCAGE
259 models.

260
261 Over Greenland, mean O₃ concentrations during the historical runs, ranged from 40 to 55 ppb
262 (Fig. 1) except in MIROC-CHEM (20-25 ppb). Similarly, Helmig et al. (2007) reported
263 annual mean of surface O₃ concentrations of 47 ppb over Greenland between 2000 and 2005,
264 particularly at the high-elevation Summit station (3200 m a.s.l.). Several investigations of
265 snow photochemical and oxidation processes over Greenland concluded that photochemical
266 O₃ production can be attributed to high levels of reactive compounds (e.g. oxidized nitrogen
267 species) present in the surface layer during the sunlit periods due to local sources e.g. NO_x
268 enhancement from snowpack emissions, peroxyacetyl nitrate (PAN) decomposition, boreal
269 forest fires or ship emissions (Granier et al., 2006; Stohl et al., 2007; Legrand et al., 2009;
270 Walker et al., 2012). PAN to NO_x ratio increases with increasing altitude and latitude (Singh
271 et al., 1992). The PAN reservoir for NO_x may be responsible for the increase in surface O₃
272 concentrations at high latitudes (Singh et al., 1992). Local O₃ production does not appear to
273 have an important contribution to the ambient high O₃ levels (Helmig et al., 2007), however

274 the long-range O₃ transport can elevate the background concentrations measured at remote
275 sites, e.g. Greenland (Ellingsen et al., 2008; Derwent et al., 2010). Low dry deposition rates
276 for O₃, from 0.01-0.05 cm s⁻¹ over oceans and snow, the downward transport of stratospheric
277 O₃, the photochemical local production and the large-scale transport (Zhang et al., 2003;
278 Legrand et al., 2009; Walker et al., 2012; Hess and Zbinden, 2013) are known factors to
279 explain higher O₃ pollution over Greenland.

280
281 The surface O₃ concentrations (> 40 ppb) and AOT40 (> 60 ppm.h) are higher over deserts,
282 downwind of O₃ precursor sources (e.g. Near East, Sierra Nevada, Colorado Desert), due to
283 lower O₃ dry deposition fluxes (Wesely and Hicks, 2000), O₃ precursors long-range transport
284 from urbanized areas and high insolation. Around the Mediterranean basin, elevated AOT40
285 values (> 60 ppm.h) are recorded, mainly due to the industrial development, road traffic
286 increment, high insolation, sea/land breeze recirculation and O₃ transport (Sicard et al., 2013).
287 All models, except MIROC-CHEM, are able to well reproduce the high surface O₃ mean
288 concentrations over Greenland and over deserts.

289
290 **Projected changes in ozone concentration and AOT40**

291
292 Recent studies display a mean global increase in background O₃ concentration from a current
293 level of 35-50 ppb (e.g. IPCC, 2014; Lefohn et al., 2014) to 55-65 ppb (e.g. Wittig et al.,
294 2007) and up to 85 ppb at NH mid-latitudes by 2100 (IPCC, 2014). During the latter half of
295 the 20th century surface O₃ concentrations have increased markedly at NH mid-latitudes (e.g.
296 Oltmans et al., 2006; Parrish et al., 2012; Paoletti et al., 2014), mainly related to increasing
297 anthropogenic precursor emissions related to economic growth of industrialized countries
298 (e.g. Lamarque et al., 2005). Our results indicate that the future projections of the mean
299 surface O₃ concentrations and AOT40 vary considerably with the different scenarios and
300 models (Fig. 1 and 2). The six models simulate a decrease of O₃ concentration by 2100 under
301 the RCP2.6 and RCP4.5 scenarios, and an increase under the RCP8.5 scenario (Lamarque et
302 al., 2011). In our study, the averaged relative changes in surface O₃ concentration means (and
303 AOT40) for the different RCPs are: -21% (-75%) for RCP2.6, - 10% (-50%) for RCP4.5 and
304 + 14% (+69%) for RCP8.5 with a strong disparity between both hemispheres, e.g. - 8% in SH
305 and - 25% in NH for RCP2.6 (Tables 3b-c). RCP8.5 is the only scenario to show an increase
306 in global background O₃ levels by 2100 (+ 23% in SH and + 11% in NH).

307

308 Under the RCP2.6 scenario, all models predict that surface O₃ will strongly decrease
309 worldwide, except in Equatorial Africa where higher O₃ levels are observed in GFDL-AM3,
310 GISS-E2-R and MOCAGE. In CESM-CAM, GFDL-AM3 and MIROC-CHEM, a
311 homogeneous decrease in O₃ burden is simulated worldwide while in GISS-E2-R, MOCAGE
312 and UM-CAM, the strongest decrease in surface O₃ mean concentrations are found where
313 high historical O₃ concentrations were reported. Under RCP4.5 scenario, the surface O₃ mean
314 concentrations and AOT40 values are lower than historical runs worldwide for all models
315 except in MOCAGE where deterioration is observed over Canada, Greenland and East Asia.
316 For all models, the surface O₃ levels and AOT40 are higher for RCP8.5 as compared to
317 historical runs and the highest increases occur in the North-western America, Greenland,
318 Mediterranean basin, Near East and East Asia. The AOT40 values, exceeding 70 ppm.h, are
319 found over the Tibetan plateau and in Near East and over Greenland. For RCP8.5, GFDL-
320 AM3 is the most pessimistic model and MIROC-CHEM the most optimistic. By the end of
321 the 21st century, similar patterns are evident for RCP4.5 compared to RCP2.6 and RCP4.5
322 simulation is intermediate between RCP2.6 and RCP8.5 ones.

323

324 For all models and RCPs, the O₃ hot-spots (mean concentrations > 50 ppb and AOT40 > 70
325 ppm.h) are over Greenland and South Asia, in particular over the Tibetan plateau. The highest
326 increases are observed in NH, in particular in North-western America, Greenland, Near East
327 and South Asia (> 65 ppb). For the three RCPs, no significant change in ground-level O₃ is
328 observed in SH and the SH extratropics makes a small contribution to the overall change.

329

330 A recent global study showed the geographical patterns of surface air temperature differences
331 for late 21st century relative to the historical run (1986-2005) in all RCP scenarios (Nazarenko
332 et al., 2015). The global warming in the RCP2.6 scenario is 2-3 times smaller than RCP4.5
333 scenario and 4-5 times smaller than RCP8.5 scenario (Nazarenko et al., 2015). For the three
334 RCPs, the greatest change is observed over the Arctic, above latitude 60°N, and in the latitude
335 band 15-45°N (IPCC, 2014; Nazarenko et al., 2015). The least warming is simulated over the
336 large area of the Southern Ocean. For RCP8.5 scenario, the global pattern of surface O₃ levels
337 and AOT40 (Fig. 1-2) is similar to surface air temperature increase distribution. For RCP8.5,
338 significant increases in air temperature are simulated over latitude 60°N and over the Tibetan
339 plateau (more than 5°C). An increase of 4-5°C over the Near East, East and South Asia, North
340 and South Africa and Canada are simulated as well as + 1-3°C for the rest of the world
341 (Nazarenko et al., 2015). The tropospheric warming is stronger in the latitude band 15-45°N

342 (Seidel et al., 2008) and Hudson et al. (2006) have demonstrated that O₃ trends over a 24-year
343 period in the NH are due to trends in the relative area of the tropics and mid-latitudes and
344 Polar Regions. If models are able to reproduce the global pattern of air temperature changes
345 distribution in agreement with surface O₃ concentrations changes.

346
347 The spread in precursor emissions (e.g. VOCs, NO_x, CO) is due to the range of representation
348 of biogenic emissions (NO_x from soils and lightning, CO from oceans and vegetation) as well
349 as the complexity of chemical schemes in particular for NMVOCs simulations (e.g. isoprene)
350 from explicitly specified to fully interactive with climate. RCP2.6 scenario has the lowest O₃
351 precursor concentrations, and RCP8.5 has relatively low NO_x, CO and VOCs emissions, but
352 very high CH₄ (Table 2b). The global emissions of NO_x (-44%), VOCs (-5%) CO (-40%) and
353 CH₄ burden (-27%) decline, while LNO_x increase by e.g. 7% under RCP2.6 (Table 2b). The
354 CO (-32%) and NO_x (-20%) emissions have decreased while LNO_x (+33%), VOCS (+1%)
355 and CH₄ burden have increased (+120%) under RCP8.5 scenario (Table 2b). The GISS-E2-R
356 model shows a greater degree of variation than other models, with a stronger increase in CH₄
357 burden (+ 153%) and in VOCs emissions (+ 20%) for RCP8.5 (Table 2b).

358
359 Excluding CH₄ burden and VOCs emissions, all the RCP scenarios include reductions and
360 redistributions of O₃ precursor emissions throughout the 21st century, due to the air pollution
361 control strategies worldwide. The changes in CH₄ burden are due to the different climate
362 policies in model assumptions. In RCP2.6, CH₄ emissions decrease steadily throughout the
363 century, in RCP4.5 it remain steady until 2050 and then decrease (Voulgarakis et al., 2013)
364 and in RCP8.5 (no climate policy) it rapidly increase compared to 2000. Methane burdens are
365 fixed in the models with no sources, except for the GISS-E2-R simulations in which surface
366 CH₄ emissions are prescribed for future rather than concentrations (Shindell et al., 2012). The
367 model chemical schemes vary greatly in their complexity, mainly due to the NMVOCs
368 simulations (Young et al., 2013). Isoprene dominates the total NMVOCs emissions (Guenther
369 et al., 1995). In contrast to other models with constant present-day isoprene emissions, the
370 GISS-ES2-R simulations incorporate climate-driven isoprene emissions, with greater BVOC
371 emissions by 2100 and a positive change in total VOCs emissions across RCPs, related to the
372 positive correlation between air temperature and isoprene emission (e.g. Guenther et al., 2006;
373 Arneth et al., 2011; Young et al., 2013).

374

375 For RCP2.6 and RCP4.5 scenarios, there is a widespread decrease in O₃ in NH by 2100. The
376 overall decrease in O₃ concentration and AOT40 means for RCP4.5 are about half of that
377 between RCP2.6 and the historical simulation. For both scenarios, the changes are dominated
378 by the decrease in O₃ precursor emissions in the NH extratropics compared to historical
379 simulations (Table 2b). In NO_x saturated areas, annual mean O₃ will slightly increase as a
380 result of a less efficient titration by NO, but the overall O₃ burden will decrease substantially
381 at hemispheric scale over time (Gao et al., 2013; Querol et al., 2014; Sicard et al., 2016a). In
382 RCP4.5, Gao et al. (2013) showed that the largest decrease in O₃ (4-10 ppb) occurs in summer
383 at mid-latitudes in the lower troposphere while the O₃ concentrations undergo an increase in
384 winter. During the warm period, the photochemistry plays a major role in the O₃ production,
385 suggesting that the reduction in surface O₃ concentrations is in agreement with the large
386 reduction in anthropogenic O₃ precursor emissions (Sicard et al., 2016a) reducing the extent
387 of regional photochemical O₃ formation (e.g. Derwent et al., 2013; Simpson et al., 2014).
388 Titration effect was also reported by Collette et al. (2012) over Europe by using six chemistry
389 transport models.

390

391 The O₃ increase can be also driven by the net impacts of climate change, i.e. increase in
392 stratospheric O₃ intrusion, changing LNO_x and impacting reaction rates, through sea surface
393 temperatures and relative humidity changes (Lau et al., 2006; Voulgarakis et al., 2013; Young
394 et al., 2013).

395

396 Under the RCP8.5 scenario, the increase in surface O₃ concentrations, by 14% on average, can
397 be attributed to the higher CH₄ emissions coupled with a strong global warming, exceeding
398 2°C, and a weakened NO titration by reducing NO_x emissions (Stevenson et al., 2013; Young
399 et al., 2013). The global CH₄ burden are 27% and 5% lower than 2000, for the RCP2.6 and
400 RCP4.5 scenarios respectively while for RCP8.5, the total CH₄ burden has more than doubled
401 compared to early 2000s and LNO_x emissions increased by 33% (Table 2b). In addition,
402 stronger increases are found over the high-elevation Himalayan Plateau reflecting increased
403 exchange with the free troposphere or stratosphere (Lefohn et al., 2012; Schnell et al., 2016).
404 Several studies reported an increase in the stratospheric O₃ influx and higher stratospheric O₃
405 levels in response to a warming climate (e.g. Hegglin and Shepherd, 2009; Zeng et al., 2010).
406 The downwards O₃ transport from the stratosphere is an important source of tropospheric O₃
407 (Hsu and Prather, 2009; Tang et al., 2011), therefore, stratospheric O₃ recovery also plays a
408 partial role (e.g. + 11% for RCP8.5) in surface O₃ burden pattern. As an example, in

409 MOCAGE, smaller reduction in global O₃ mean concentrations (-13%) and higher increase in
410 stratospheric O₃ inputs (+20%) are observed for RCP2.6 (Table 3b). Similarly, for RCP8.5,
411 the highest increase in O₃ mean concentrations (+23%) and stratospheric O₃ (+24%) are
412 recorded in MOCAGE. In addition, lightning NO_x emissions show significant upward trend
413 from 2000 to 2100, in particular for the strongest warming scenario (RCP8.5) with greater
414 convective and lightning activity (e.g. Williams, 2009; Lamarque et al., 2013). For RCP8.5, a
415 reduction in surface O₃ concentrations is also simulated over the equatorial region, where the
416 increased relative humidity, in a warmer climate, increases the O₃ loss rate (e.g. Johnson et
417 al., 1999; Zeng and Pyle, 2003).

418

419 **Risk areas for vegetation under RCP scenarios**

420

421 Figure 3 shows the changes in the potential O₃ impact on photosynthetic carbon assimilation
422 between present and future. It should be noted that a zero percentage of change (i.e. no
423 change) for IO₃, is simulated in sparsely vegetated regions (e.g. Gobi, Sahara, Near East,
424 Western plateau and Greenland), while the change can be higher than 100% when the
425 historical O₃ concentrations are lower than 40 ppb (i.e. AOT40 = 0 and IO₃ = 0) and the O₃
426 concentrations exceed 40 ppb under RCPs (i.e. AOT40 > 0, IO₃ > 0).

427

428 The potential O₃ impact for vegetation strongly decreases in NH for RCP2.6, except in
429 MOCAGE where a slight increase in the risk factor (+ 15 %) is simulated at high latitudes and
430 in South Asia. Conversely, the areas where the risk for vegetation increases (> 60 %) occur
431 over Africa (+ 15% to + 60%) for all models, except in CESM-CAM where no change is
432 observed across Africa. Under RCP4.5 scenario, the strongest increase in potential risk for
433 vegetation (> + 60 %) is simulated by MOCAGE, markedly different from the other models,
434 above the latitude 50°N. For all models, the potential O₃ impact for vegetation increases
435 across Africa, from - 15% to + 60% while slight decreases or no change occur worldwide.
436 Under RCP8.5 scenario, an increase of average O₃ over a significant part of the domain is
437 simulated, therefore the exposure to O₃ pollution and impacts on vegetation will increase
438 worldwide by 2100. An increase of the O₃ impacts on vegetation is simulated in Northern
439 U.S., South America, Asia and Africa while a reduction in particular over Eastern U.S. and
440 Southeastern China, and a slight increase (+ 15%) or decrease (- 15%) over Europe depending
441 on the model, are simulated.

442 In summary, compared to the historical simulations, the averaged relative changes in the O₃
443 risk factor for the different RCPs are: - 61% for RCP2.6, - 47% for RCP4.5 and + 70% for
444 RCP8.5 (Table 3d). We thus find a significant reduction in risk for vegetation for both
445 RCP2.6 and RCP4.5 scenarios, except in South Africa and at high-latitudes in MOCAGE
446 simulations, and a strong increase in global risk under RCP8.5. Under RCP2.6 and RCP4.5
447 scenarios, IO₃ slightly increases in Africa and over North America and Asia (> latitude 60°N)
448 in MOCAGE. The risk increases over the few areas where the O₃ concentrations increased
449 between the historical period and 2100. Under both scenarios, the strongest reductions in risk
450 are observed over Amazon, Central Africa and South Asia, i.e. where the O₃ concentrations
451 have strongly declined between historical period and 2100. Under the RCP8.5, the areas
452 where the highest projected O₃ mean concentrations are simulated (e.g. Greenland, deserts)
453 are not associated with an increase in IO₃ due to the absence of vegetation. Under RCP8.5,
454 IO₃ increases worldwide while a reduction is simulated over Southeast North America,
455 northern Amazon, Central Africa and Southeast Asia, and a slighter reduction or a slight
456 increase is simulated over Western Europe (depending on the model).

457

458 The spatial pattern of IO₃ is consistent with previous analyses on global environmental
459 changes (climate, land-cover, nitrogen deposition, CO₂ fertilization) impacts on vegetation
460 (Nemani et al., 2003; Zhu et al., 2016), i.e. the highest reduction in risk for vegetation, in
461 particular under RCP8.5, occurs over areas where a strong increase in greening, LAI and NPP
462 is observed due to global changes and where a reduction in surface O₃ mean concentrations is
463 found by 2100 (Fig. 1). The regions with the largest greening trends are in Southeast North
464 America, northern Amazon, Europe, Central Africa and Southeast Asia with an average
465 increase of the observed LAI exceeding 0.25 m² m⁻² per year (Zhu et al., 2016). The CO₂
466 fertilization effects (70%), nitrogen deposition (9%) and climate change (8%) explain the
467 observed greening trend (Zhu et al., 2016). The changing climate alone produces persistent
468 NPP increases and the regions with the highest increase in NPP, ranging from 1.0-1.5% per
469 year, are in Southeast North America, northern Amazon, Western Europe, Central Africa and
470 South Asia (Nemani et al., 2003). From 1982 to 1999, the highest increases are observed in
471 tropical regions, with more than 1.5% per year over Amazon rainforest which accounts for
472 42% of the global NPP increase (Nemani et al., 2003). Amazon rainforest is one region where
473 the effects are statistically significant. This is particularly important owing to the role of the
474 Amazon rainforests in the global carbon cycle (Zhu et al., 2016). In these areas, we observed a
475 strong increase in NPP and LAI due to warming climate while a reduction in GPP (from - 10

476 to - 20%) due to O₃ is observed (Sitch et al., 2007). Inversely, the risk for vegetation IO₃
477 increases in particular in Africa, e.g. western Africa along the Gulf of Guinea, in South Brazil
478 and over high-latitudes regions (> 60°N) in North America and Asia where a reduction or a
479 slight increase in LAI (from - 0.05 to + 0.03 m² m⁻² per year) and strong decreases in NPP
480 (1.0-1.5% per year) are simulated (Nemani et al., 2003; Zhu et al., 2016).

481

482 Sitch et al. (2007) reported a high GPP reduction due to O₃ effects, between 1901 and 2100
483 under the *Special Report on Emissions Scenarios A2 emissions* scenario, exceeding 30% in
484 summer over Western Europe, Eastern North America, Amazon, central Africa and South
485 Asia. Previous studies reported that the reductions in GPP simulated by Sitch et al. (2007) are
486 overestimated up to six times due to i) the lack of empirical data about the response of
487 different species to O₃, Sitch et al. (2007) focused on broad-leaved tree, needle-leaved tree, C3
488 crops, C4 crops and shrubs; ii) the fact that a few experiments have shown no response, e.g.
489 grasslands (Bassin et al., 2013) and iii) the non-inclusion of the nitrogen limitation of growth
490 (Ren et al., 2011; Zak et al., 2011; Kvaleveg and Myhre 2013). In addition, the simulated O₃
491 concentrations over Amazon forest exceed 90 ppb in summer in Sitch et al. (2007) while the
492 annual O₃ mean is around 15-20 ppb by 2100 in our study.

493

494 The projected land covers widely vary under RCPs (Betts et al., 2015). In RCP2.6 scenario,
495 the ground surface covered by croplands increases as a result of bio-energy production, with a
496 more-or-less constant use of grassland. The RCP4.5 scenario focuses on global reforestation
497 programs as part of global climate policy, as a result, the use of cropland and grassland
498 decreases. Under RCP8.5, an increase in croplands and grasslands is applied mostly driven by
499 an increasing global population (van Vuuren et al., 2011). About 50% of forests, grasslands
500 and croplands might be exposed to high O₃ levels by the end of the 21st century (Sitch et al.,
501 2007; Wittig et al., 2009).

502 Based on a comparison between Figure 2 and the Global Land Cover Facility maps, we can
503 observe that generally the AOT40, i.e. the potential O₃ risk to vegetation is high over
504 shrublands (e.g. high-latitude region), broadleaf forests (e.g. central Africa), needleleaf forests
505 (e.g. North America) and crops (e.g. South Asia). Under RCP2.6 and RCP4.5, the risk
506 decreases over areas covered by shrublands, savannas and slightly decreases over areas with
507 needleleaf forests in Northern America and Northern Asia. The risk strongly increases over
508 broadleaf forest in Africa and the risk slightly decreases or slightly increases over grasslands

509 (Central Asia and central Africa and U.S.). Under RCP8.5, the largest decreases in risks occur
510 in Eastern U.S., Europe and South-eastern China, where the ground is mainly dominated by
511 croplands, in all models except CESM-CAM.

512 **Conclusions**

513 From six global atmospheric chemistry transport models, we illustrate the changes, i.e.
514 differences for late 21st century relative to the historical run, in ground-level O₃
515 concentrations and vegetation impact metric (AOT40). Finally, the potential O₃ impacts on
516 photosynthetic carbon assimilation worldwide are investigated to define potential risk areas
517 for vegetation at global scale by 2100. A major advantage of this study is a comparison
518 between models and scenarios to explore future potential O₃ impacts.

519
520 The six models are able to well reproduce the spatial pattern of historical O₃ concentration
521 and AOT40 at global scale, in particular GISS-E2-R and MOCAGE are able to simulate the
522 higher O₃ levels in areas downwind of precursor sources and at the high-elevation areas. The
523 model outputs emphasize the strong asymmetry in the tropospheric O₃ distribution between
524 NH and SH; substantially higher O₃ mean concentrations are observed in the NH (ca. 38 ppb),
525 particularly in the latitude band 15-45°N, than in the SH (ca. 23 ppb). The natural emissions
526 of O₃ precursors (e.g. lightning NO_x, CO from oceans, isoprene) as well as the complexity of
527 chemical schemes are significant sources of model-to-model differences.

528
529 In this study, the projected mean surface O₃ concentrations and AOT40 dependent on global
530 and regional emission pathways. Compared to early 2000s, the results suggest changes in
531 surface O₃ of -9.5 ± 2.0 ppb (NH) and -1.8 ± 2.1 ppb (SH) in the cleaner RCP2.6 scenario
532 and of $+4.4 \pm 2.8$ ppb (NH) and $+5.1 \pm 2.1$ ppb (SH) in RCP8.5 scenario. For RCP2.6 and
533 RCP4.5, absolute decreases are observed for the Mediterranean basin and the Western U.S.
534 due to less precursor emissions in the NH extratropics (e.g. reduction of 5-7 ppb over
535 Europe). Smaller reduction in surface O₃ levels in South and East Asia highlight the smaller
536 changes in O₃ precursor emissions due to the recent emission growth in this region (e.g.
537 Zhang et al., 2009; Xing et al., 2015). For RCP8.5, all models show climate-driven increases
538 in ground-level O₃ in particular over the Western U.S, Greenland, South Asia and Northeast
539 China. The changes in surface O₃ over North America and Europe ranged from + 1-5 ppb
540 under RCP8.5. South Asia sees the greatest increase, up to more than 10 ppb for RCP 8.5.
541 This O₃ increase can be attributed to substantial increase in CH₄ emissions coupled with a

542 strong global warming, exceeding 2°C, and a weakened NO titration and a greater
543 stratospheric O₃ influx (Kawase et al., 2011; Wild et al., 2012; Young et al., 2013). A decline
544 in CH₄ emissions will undoubtedly benefit future O₃ control.

545

546 Most important results from the study are the spatial patterns and projected changes in global
547 AOT40 and risk areas for vegetation under the RCP scenarios. Even if AOT40 was computed
548 year-round, the global models suggest that AOT40-based critical levels for the protection of
549 forests and crops will be exceeded over many areas of the NH, and in parts of North America,
550 East and South Asia, and they may be exceeded by a factor exceeding 10 under RCP8.5.
551 AOT40 was used widely during the last two decades, not only in Europe but also in South
552 America (Moura et al., 2014) and Asia (Hoshika et al., 2011) when environmental factors are
553 not limiting, e.g. water availability, air temperature, solar radiation affecting stomata opening
554 (Anav et al., 2016; De Marco et al., 2016). As a result, the flux-based metric is introduced as
555 new standard for vegetation protection against effects of O₃, taking into account the
556 modifying effects of multiple climatic and phenological factors on O₃ uptake (Paoletti and
557 Manning, 2007; Sicard et al., 2016b,c).

558 Ozone may be a major threat to biodiversity over large regions of the world (Sicard et al.,
559 2016b), however the size of these areas remains uncertain. The potential O₃ impact on carbon
560 assimilation, IO₃, provides a clear indicator of the potential risk to vegetation. By 2100, the
561 potential O₃ impact on photosynthetic carbon assimilation decreases by 61% and 47% under
562 RCP2.6 and RCP4.5, respectively and increases by 70% under RCP8.5, compared to early
563 2000s over the whole domain. The potential risk areas for vegetation vary worldwide
564 according to the dominant vegetation cover. The strongest increase of the O₃ impacts on
565 vegetation is simulated in Northern America and Asia and central Africa. The highest
566 reduction in risk for vegetation (i.e. Southeast North America, the northern Amazon, Central
567 Africa and Southeast Asia) occurs over areas where a strong increase in greening, LAI and
568 NPP is observed and where a reduction in O₃ mean concentrations is found by 2100. Generally,
569 deciduous broadleaf are highly O₃-sensitive risk areas, grasslands and needleleaf forests are
570 moderately O₃-sensitive risk areas. Crops are more sensitive to O₃ exposure than trees and
571 deciduous trees are more sensitive than coniferous trees with lower stomatal conductance
572 (Felzer et al., 2004; Ren et al., 2007; Wittig et al., 2009; Anav et al., 2011).

573 Many ecosystems worldwide are unprotected from O₃ due to the lack of international efforts
574 (Emberson et al., 2014). An efficient reduction in overall O₃ levels is expected over North

575 America and Europe in all RCP scenarios and worldwide if CH₄ emissions are reduced (e.g.
576 Kirtman et al., 2013; Pfister et al., 2014; Schnell et al., 2016). To efficiently protect vegetation
577 against O₃ pollution, suitable standards taking into account the detoxification processes (e.g.
578 flux-based metric) are urgently needed and the mitigation actions must be as part of
579 international emission reduction programmes.

580

581 **Acknowledgements**

582 This work was carried out with the contribution of the LIFE financial instrument of the
583 European Union (LIFE15 ENV/IT/183) in the framework of the MOTTLES project
584 “Monitoring ozone injury for setting new critical levels” and published within the
585 International Union of Forest Research Organizations (IUFRO) Task Force on Climate
586 Change and Forest Health and IUFRO RG 7.01.09 “Ground-level ozone”.

587

588 **Bibliographic references**

- 589 **Ainsworth E.A.**, Yendrek C.R., Sitch S., Collins, W.J., Emberson L.D., 2012, “The effect of
590 Tropospheric Ozone on Net Primary Productivity and Implications for Climate Change”.
591 *Annu. Rev. Plant Biol.* 63: 637-661
- 592 **Anav A.**, Menut L., Khvorostyanov D., Viovy N., 2011, “Impact of tropospheric ozone on the
593 Euro-Mediterranean vegetation”. *Global Change Biol.* 17: 2342-2359
- 594 **Arbaugh M.J.**, and Bytnerowicz A., 2003, “Ambient ozone patterns and effects over the
595 Sierra Nevada: synthesis and implications for future research”. In: A. Bytnerowicz, M.
596 Arbaugh, R. Alonso (eds), *Ozone Air Pollution in the Sierra Nevada: Distribution and Effects*
597 *on Forests, Developments in Environmental Science*, vol. 2, Elsevier, Amsterdam, 249-261
- 598 **Arneth A.**, Schurgers G., Lathière J., Duhl T., Beerling D. J., et al., 2011, “Global terrestrial
599 isoprene emission models: sensitivity to variability in climate and vegetation”. *Atmos. Chem.*
600 *Phys.* 11: 8037-8052
- 601 **Arneth A.**, Schurgers G., Hickler T., Miller P.A., 2008, “Effects of species composition, land
602 surface cover, CO₂ concentration and climate on isoprene emissions from European forests”.
603 *Plant Biol.* 10: 150-162
- 604 **Ashmore M.R.**, 2005, “Assessing the future global impacts of ozone on vegetation”. *Plant*
605 *Cell Environ.* 28: 949-964
- 606 **Ashworth K.**, Wild O., Hewitt C.N., 2013, “Impacts of biofuel cultivation on mortality and
607 crop yields”. *Nat. Clim. Change* 3: 492-496
- 608 **Bassin S.**, Volk M., Fuhrer J., 2013, “Species composition of subalpine grassland is sensitive
609 to nitrogen deposition, but not ozone, after seven years of treatment”. *Ecosystems* 16: 1105-
610 1117
- 611 **Betts R.A.**, Golding N., Gonzalez P., Gornall J., Kahana R., et al., 2015, “Climate and land
612 use change impacts on global terrestrial ecosystems and river flows in the HadGEM2-ES
613 Earth system model using the representative concentration pathways”. *Biogeosciences* 12:
614 1317-1338
- 615 **Bian J.**, Yan R., Chen H., Lü D., Massie S.T., 2011, “Formation of the summertime ozone
616 valley over the Tibetan Plateau: The Asian summer monsoon and air column variations”.
617 *Adv. Atmos. Sci.* 28: 1318-1325
- 618 **Bowman K.W.**, Shindell D.T., Worden H.M., Lamarque J.F., Young P.J., 2013, “Evaluation
619 of ACCMIP outgoing longwave radiation from tropospheric ozone using TES satellite
620 observations”. *Atmos. Chem. Phys.* 13: 4057-4072
- 621 **Clifton O.E.**, Fiore A.M., Correa G., Horowitz L.W., Naik V., 2014, “Twenty-first century
622 reversal of the surface ozone seasonal cycle over the northeastern United States”. *Geophys.*
623 *Res. Lett.* 41: 7343-7350
- 624 **Chen X.L.**, Ma Y.M., Kelder H., Su Z., Yang K., 2011, “On the behaviour of the tropopause
625 folding events over the Tibetan Plateau”. *Atmos. Chem. Phys.* 11: 5113-5122
- 626 **Chevalier A.**, Gheusi F., Delmas R., Ordóñez C., Sarrat C., et al., 2007, “Influence of altitude
627 on ozone levels and variability in the lower troposphere: a ground-based study for Western
628 Europe over the period 2001-2004”. *Atmos. Chem. Phys.* 7: 4311-4326
- 629 **Colette A.**, Granier C., Hodnebrog Ø., Jakobs H., Maurizi A., et al., 2012, “Future air quality
630 in Europe: a multi-model assessment of projected exposure to ozone”. *Atmos. Chem. Phys.*
631 12: 10613-10630
- 632 **Cooper O.R.**, Parrish D.D., Ziemke J., Balashov N.V., Cupeiro M., 2014, “Global
633 distribution and trends of tropospheric ozone: An observation-based review”. *Elementa:*
634 *Science of the Anthropocene* 2: 000029
- 635 **Cooper O.R.**, Sweeney C., Gao R.S., Tarasick D., Leblanc T., 2012, “Long-term ozone
636 trends at rural ozone monitoring sites across the United States, 1990-2010”. *J. Geophys. Res.*
637 117: D22307

638 **Cubasch U.**, Wuebbles D., Chen D., Facchini M.C., Frame D., et al., 2013, “Introduction, in
639 Climate Change 2013: The Physical Science Basis”. Contribution of Working Group I to the
640 Fifth Assessment Report of the Intergovernmental Panel on Climate Change, edited by T. F.
641 Stocker et al., Cambridge Univ. Press, Cambridge, U. K. and New York

642 **De Marco A.**, Sicard P., Vitale M., Carriero G., Renou C., et al., 2015, “Metrics of ozone risk
643 assessment for Southern European forests: canopy moisture content as a potential plant
644 response indicator”. *Atmos. Environ.* 120: 182-190

645 **Derwent R.G.**, Utembe S.R., Jenkin M.E., Shallcross D.E., 2015, “Tropospheric ozone
646 production regions and the intercontinental origins of surface ozone over Europe”. *Atmos.*
647 *Environ.* 112: 216-224

648 **Derwent R.G.**, Manning A.J., Simmonds P.G., Spain T.G., O'Doherty S., 2013, “Analysis
649 and interpretation of 25 years of ozone observations at the Mace Head Atmospheric Research
650 Station on the Atlantic Ocean coast of Ireland from 1987 to 2012”. *Atmos. Environ.* 80: 361-
651 368

652 **Derwent R.G.**, Witham C.S., Utembe S.R., Jenkin M.E., Passant N.R., 2010, “Ozone in
653 Central England: the impact of 20 years of precursor emission controls in Europe”. *Environ.*
654 *Sci. Policy* 13: 195-204

655 **Donner L.J.**, Wyman B.L., Hemler R.S., Horowitz L.W., Ming Y., et al., 2011, “The
656 dynamical core, physical parameterizations, and basic simulation characteristics of the
657 atmospheric component AM3 of the GFDL Global Coupled Model CM3”. *J. Climate* 24:
658 3484-3519

659 **European Environment Agency**, 2015 “Air quality in Europe - 2015 report”. ISBN 978-92-
660 9213-702-1. Report No 5/2015

661 **Ellingsen K.**, Gauss M., Van Dingenen R., Dentener F.J., Emberson L., et al., 2008, “Global
662 ozone and air quality: a multi-model assessment of risks to human health and crops”. *Atmos.*
663 *Chem. Phys.* 8: 2163-2223

664 **Emberson L.D.**, Fuhrer J., Ainsworth L., Ashmore M.R., 2014, “Biodiversity and Ground-
665 level Ozone”. Report UNEP/CBD/SBSTTA/18/INF/17. Convention on Biological Diversity,
666 18th meeting, Montreal, 23-28 June 2014

667 **Fares S.**, Vargas R., Detto M., Goldstein A.H., Karlik J., et al., 2013, “Tropospheric ozone
668 reduces carbon assimilation in trees: estimates from analysis of continuous flux
669 measurements”. *Global Change Biol.* 19: 2427-2443

670 **Federal Register**, 2015, “National Ambient Air Quality Standards for Ozone”. 40 CFR Part
671 50, 51, 52, 53, and 58, pp 65292-65468

672 **Felzer B.S.F.**, Kicklighter D.W., Melillo J.M., Wang C., Zhuan Q., et al., 2004, “Ozone
673 effects on net primary production and carbon sequestration in the conterminous United States
674 using a biogeochemistry model”. *Tellus B* 56: 230-248

675 **Fiore A.M.**, Naik V., Leibensperger E.M., 2015, “Air quality and climate connections”. *J. Air*
676 *Waste Manage. Assoc.* 65: 645-685

677 **Fiore A.M.**, Naik V., Spracklen D.V., Steiner A., Unger N. et al., 2012, “Global air quality
678 and climate”. *Chem. Soc. Rev.* 41: 6663-6683

679 **Fiscus E.L.**, Booker F.L., Burkey K.O., 2005, “Crop responses to ozone: uptake, modes of
680 action, carbon assimilation and partitioning”. *Plant Cell Environ.* 28: 997-1011

681 **Gao Y.**, Fu J.S., Drake J.B., Lamarque J.F., Liu Y., 2013, “The impact of emission and
682 climate change on ozone in the United States under representative concentration pathways
683 (RCPs)”. *Atmos. Chem. Phys.* 13: 9607-9621

684 **Granier C.**, Niemeier U., Jungclaus J.H., Emmons L., Hess P., et al., 2006, “Ozone pollution
685 from future ship traffic in the Arctic northern passages”. *Geophys. Res. Lett.* 33, doi:
686 10.1029/2006GL026180

687 **Guenther A.B.**, Karl T., Harley P., Wiedinmyer C., Palmer P.I., Geron C., 2006, “Estimates
688 of global terrestrial isoprene emissions using MEGAN (Model of Emissions of Gases and
689 Aerosols from Nature)”. *Atmos. Chem. Phys.* 6: 3181-3210

690 **Guenther A.B.**, Hewitt C.N., Erickson D., Fall R., Geron, C., et al., 1995, “A global model of
691 natural volatile organic compound emissions”. *J. Geophys. Res.* 100: 8873-8892

692 **Guo D.**, Su Y., Shi C., Xunn J., Powell Jr. A.M., 2015, “Double core of ozone valley over the
693 Tibetan Plateau and its possible mechanisms”. *Journal of Atmospheric and Solar-Terrestrial*
694 *Physics* 130: 127-131

695 **Hegglin M.I.** and Shepherd T.G., 2009, “Large climate-induced changes in ultraviolet index
696 and stratosphere-to-troposphere ozone flux”. *Nature Geosci.* 2: 687

697 **Helmig D.**, Oltmans S.J., Morse T.O., Dibb J.E., 2007, “What is causing high ozone at
698 Summit, Greenland?”. *Atmos. Environ.* 41: 5031-5043

699 **Hess P.G.** and Zbinden R., 2013, “Stratospheric impact on tropospheric ozone variability and
700 trends: 1990-2009”. *Atmos. Chem. Phys.* 13: 649-674

701 **Holland M.**, Kinghorn S., Emberson L., Cinderby S., Ashmore M., et al., 2006,
702 “Development of a framework for probabilistic assessment of the economic losses caused by
703 ozone damage to crops in Europe”. UNECE International Cooperative Programme on
704 Vegetation. Contract Report EPG 1/3/205. CEH Project No: C02309NEW

705 **Hoshika Y.**, Shimizu Y., Omasa K., 2011, “A comparison between stomatal ozone uptake
706 and AOT40 of deciduous trees in Japan”. *iForest – Biogeosciences and Forestry* doi:
707 10.3832/ifor0573-004

708 **Hsu J.** and Prather M.J., 2009, “Stratospheric variability and tropospheric ozone”. *J.*
709 *Geophys. Res.* 114: D06102

710 **Hu X.M.**, Klein Petra M., Xue M. et al., 2013, “Impact of the vertical mixing induced by low-
711 level jets on boundary layer ozone concentration”. *Atmos. Environ.* 70: 123-130

712 **Hudson R.D.**, Andrade M.F., Follette M.B., Frolov A.D., 2006, “The total ozone field
713 separated into meteorological regimes – Part II: Northern Hemisphere mid-latitude total ozone
714 trends”. *Atmos. Chem. Phys.* 6: 5183-5191

715 **IPCC**, Intergovernmental Panel on Climate Change, 2014, “Summary for Policymakers”. In:
716 “Climate Change 2014: Impacts, Adaptation and Vulnerability”. Contribution of Working
717 Group II to the Fifth Assessment Report of the Intergovernmental Panel on Climate Change.
718 Cambridge University Press, Cambridge, UK

719 **Jeričević A.**, Koračin D., Jiang J., Chow J., Watson J., et al., 2013, “Air Quality Study of
720 High Ozone Levels in South California”. Part of the series NATO Science for Peace and
721 Security Series C: Environmental Security. *Air Pollution Modeling and its Application XXII:*
722 629-633

723 **Johnson C.E.**, Collins W.J., Stevenson D.S., Derwent R.G., 1999, “Relative roles of climate
724 and emissions changes on future tropospheric oxidant concentrations”. *J. Geophys. Res.* 104:
725 18631-18645

726 **Josse B.**, Simon P., Peuch V.H., 2004, “Radon global simulations with the multiscale
727 chemistry and transport model MOCAGE”. *Tellus-B* 56: 339-356

728 **Kawase H.**, Nagashima T., Sudo K., Nozawa T., 2011, “Future changes in tropospheric
729 ozone under Representative Concentration Pathways (RCPs)”. *Geophys. Res. Lett.* 38:
730 L05801

731 **Kelly J.**, Makar P.A., Plummer D.A., 2012, “Projections of mid-century summer air-quality
732 for North America: effects of changes in climate and precursor emissions”. *Atmos. Chem.*
733 *Phys.* 12: 5367-5390

734 **Kirtman B.**, Power S.B., Adedoyin J.A., Boer G.J., Bojariu R., et al., 2013, “Near-term
735 climate change: Projections and predictability, in *Climate Change 2013: The Physical Science*
736 *Basis*”. Contribution of Working Group I to the Fifth Assessment Report of the

737 Intergovernmental Panel on Climate Change, edited by T.F. Stocker et al., Cambridge Univ.
738 Press, Cambridge, U. K., and New York

739 **Klingberg J.**, Engardt M., Karlsson P.E., Langner J., Pleijel H., 2014, “Declining ozone
740 exposure of European vegetation under climate change and reduced precursor emissions”.
741 *Biogeosciences* 11: 5269-5283

742 **Krinner G.**, Viovy N., de Noblet-Ducoudré N., Ogée J., Polcher J., et al., 2005, “A dynamic
743 global vegetation model for studies of the coupled atmosphere-biosphere system”. *Global*
744 *Biogeochem. Cy.* 19: GB1015

745 **Kulkarni P.S.**, Bortoli D., Domingues A., Silva A.M., 2015, “Surface Ozone Variability and
746 Trend over Urban and Suburban Sites in Portugal”. *Aerosol Air Qual. Res.*: 1-15

747 **Kulkarni P.S.**, Bortoli D., Salgado R., Anton M., Costa M.J., et al., 2011, “Tropospheric
748 ozone variability over the Iberian Peninsula”. *Atmos. Environ.* 45: 174-182

749 **Kvalevag M.M.** and Myrhe G., 2013, “The effect of carbon-nitrogen coupling on the reduced
750 land carbon sink caused by ozone”. *Geophys. Res. Lett.* 40: 3227-3231

751 **Lamarque J.F.**, Shindell D.T., Josse B., Young P.J., Cionni I., et al., 2013, “The
752 Atmospheric Chemistry and Climate Model Intercomparison Project (ACCMIP): overview
753 and description of models, simulations and climate diagnostics”. *Geosci. Model Dev.* 6: 179-
754 206

755 **Lamarque J.F.**, Emmons L.K., Hess P.G., Kinnison D.E., Tilmes, S., et al., 2012, “CAM-
756 chem: description and evaluation of interactive atmospheric chemistry in the Community
757 Earth System Model”. *Geosci. Model Dev.* 5: 369-411

758 **Lamarque J.F.**, Bond T.C., Eyring V., Granier C., Heil A., et al., 2010, “Historical (1850–
759 2000) gridded anthropogenic and biomass burning emissions of reactive gases and aerosols:
760 methodology and application”. *Atmos. Chem. Phys.* 10: 7017-7039

761 **Lamarque J.F.**, Hess P.G., Emmons L.K., Buja L.E., Washington W.M., Granier C., 2005,
762 “Tropospheric ozone evolution between 1890 and 1990”. *J. Geophys. Res.* 110: D08304

763 **Langner J.**, Engardt M., Baklanov A., Christensen J.H., Gauss M., et al., 2012, “A multi-
764 model study of impacts of climate change on surface ozone in Europe”. *Atmos. Chem. Phys.*
765 12: 10423-10440

766 **Lau N.C.**, Leetmaa A., Nath M.J., 2006, “Attribution of atmospheric variations in the 1997-
767 2003 period to SST anomalies in the Pacific and Indian Ocean basins”. *J. Climate* 19: 3607-
768 3628

769 **Lee Y.H.** and Adams P.J., 2011, “A fast and efficient version of the two-moment aerosol
770 sectional (TOMAS) global aerosol microphysics model”. *Aerosol Sci. Tech.* 46: 678-689

771 **Lefohn A.S.**, Malley C.S., Simon H., Wells B., Xu X., et al., 2017, “Responses of human
772 health and vegetation exposure metrics to changes in ozone concentration distributions in the
773 European Union, United States, and China”. *Atmos. Environ.* 152: 123-145

774 **Lefohn A.S.**, Emery C., Shadwick D., Wernli H., Jung J., Oltmans S.J., 2014, “Estimates of
775 background surface ozone concentrations in the United States based on model-derived source
776 apportionment”. *Atmos. Environ.* 84:275-288.

777 **Lefohn A.S.**, Wernli H., Shadwick D., Oltmans S.J., Shapiro M., 2012, “Quantifying the
778 frequency of stratospheric-tropospheric transport affecting enhanced surface ozone
779 concentrations at high- and low-elevation monitoring sites in the United States”. *Atmos.*
780 *Environ.* 62: 646-656

781 **Lefohn A.S.**, Shadwick D., Oltmans S.J., 2010, “Characterizing changes in surface ozone
782 levels in metropolitan and rural areas in the United States for 1980-2008 and 1994-2008”.
783 *Atmos. Environ.* 44: 5199-5210

784 **Legrand M.**, Preunkert S., Jourdain B., Gallée H., Goutail F., et al., 2009, “Year-round record
785 of surface ozone at coastal (Dumont d’Urville) and inland (Concordia) sites in East
786 Antarctica”. *J. Geophys. Res.* 114: doi: 10.1029/2008JD011667

787 **Liu C.**, Liu Y., Cai Z., Gao S., Bian J., et al., 2010, “Dynamic formation of extreme ozone
788 minimum events over the Tibetan Plateau during northern winters 1987-2001”. *J. Geophys.*
789 *Res.* 115: D18311

790 **Meinshausen M.**, Wigley T.M.L., Raper S.C.B., 2011, “Emulating atmosphere-ocean and
791 carbon cycle models with a simpler model, MAGICC6 - Part 2: Applications”. *Atmos. Chem.*
792 *Phys.* 11: 1457-1471

793 **Mills G.**, Hayes F., Simpson D., Emberson L., Norris D., et al., 2011, “Evidence of
794 widespread effects of ozone on crops and (semi-)natural vegetation in Europe (1990-2006) in
795 relation to AOT40 and flux-based risk maps”. *Global Change Biol.* 17: 592-613

796 **Monks P.S.**, Archibald A.T., Colette A., Cooper O., Coyle M., et al., 2015, “Tropospheric
797 ozone and its precursors from the urban to the global scale from air quality to short-lived
798 climate forcer”. *Atmos. Chem. Phys.* 15: 8889-8973

799 **Moura B.B.**, Alves E.S., de Souza S.R., Domingos M., Vollenweider P., 2014, “Ozone
800 phytotoxic potential with regard to fragments of the Atlantic Semi-deciduous Forest
801 downwind of Sao Paulo, Brazil”. *Environ. Pollut.* 192: 65-73

802 **Myhre G.**, Shindell D., Bréon F.M., Collins W., Fuglestedt J., et al., 2013, “Anthropogenic
803 and Natural Radiative Forcing”. In: *Climate Change 2013: The Physical Science Basis.*
804 *Contribution of Working Group I to the Fifth Assessment Report of the Intergovernmental*
805 *Panel on Climate Change.* Cambridge University Press, Cambridge, United Kingdom and
806 New York, USA

807 **Naik V.**, Voulgarakis A., Fiore A.M., Horowitz L.W., Lamarque J.F., et al., 2012,
808 “Preindustrial to present day changes in tropospheric hydroxyl radical and methane lifetime
809 from the Atmospheric Chemistry and Climate Model Intercomparison Project (ACCMIP)”.
810 *Atmos. Chem. Phys. Discuss.* 12: 30755-30804

811 **Nazarenko L.**, Schmidt G.A., Miller R.L., Tausnev N., Kelley M., et al., 2015, “Future
812 climate change under RCP emission scenarios with GISS ModelE2”. *J. Adv. Model. Earth*
813 *Syst.* 7: 244-267

814 **Nemani R.R.**, Keeling C.D., Hashimoto H., Jolly W.M., Piper S.C., et al., 2003, “Climate-
815 Driven Increases in Global Terrestrial Net Primary Production from 1982 to 1999”. *Science*
816 300: 1560-1563

817 **Ollinger S.V.**, Aber J.D., Reich P.B., 1997, “Simulating ozone effects on forest productivity:
818 interactions among leaf, canopy, and stand-level processes”. *Ecol. Appl.* 7: 1237-1251.

819 **Oltmans S.J.**, Lefohn A.S., Harris J.M., Galbally I., Scheel H.E., et al., 2006, “Long-term
820 changes in tropospheric ozone”. *Atmos. Environ.* 40: 3156-3173

821 **Paoletti E.**, De Marco A., Beddows D.C.S., Harrison R.M., Manning W.J., 2014, “Ozone
822 levels in European and USA cities are increasing more than at rural sites, while peak values
823 are decreasing”. *Environ. Pollut.* 192: 295-299

824 **Paoletti E.** and Manning W.J., 2007, “Toward a biologically significant and usable standard
825 for ozone that will also protect plants”. *Environ. Pollut.* 150: 85-95

826 **Paoletti E.**, 2006, “Impact of ozone on Mediterranean forest: A review”. *Environ. Pollut.* 144:
827 463-474

828 **Parrish D.D.**, Law K.S., Staehelin J., Derwent R., Cooper O.R., et al., 2012, “Long-term
829 changes in lower tropospheric baseline ozone concentrations at northern mid-latitudes”.
830 *Atmos. Chem. Phys.* 12: 11485-11504

831 **Pfister G.G.**, Walters S., Lamarque J.F., Fast J., Barth M.C., et al., 2014, “Projections of
832 future summertime ozone over the U.S”. *J. Geophys. Res. Atmos.* 119: 5559-5582

833 **Price C.** and Rind D.H., 1992, “A simple lightning parameterization for calculating global
834 lightning distributions”. *J. Geophys. Res.*, 97: 9919-9933

835 **Proietti C.**, Anav A., De Marco A., Sicard P., Vitale M., 2016, “A multi-sites analysis on the
836 ozone effects on Gross Primary Production of European forests”. *Sci. Total Environ.* 556: 1-
837 11

838 **Querol X.**, Alastuey A., Pandolfi M., Reche C., Pérez N., et al., 2014, “2001-2012 trends on
839 air quality in Spain”. *Sci. Total Environ.* 490: 957-969.

840 **Reich P.B.**, 1987, “Quantifying plant response to ozone: a unifying theory”. *Tree Physiol.* 3:
841 63-91

842 **Ren W.**, Tian H., Liu M., Zhang C., Chen G., et al., 2007, “Effects of tropospheric ozone
843 pollution on net primary productivity and carbon storage in terrestrial ecosystems of China”.
844 *J. Geophys. Res.* 112: 1-17

845 **Riahi K.**, Rao S., Krey V., Cho C., Chirkov V., et al., 2011, “RCP 8.5 - A scenario of
846 comparatively high greenhouse gas emissions”. *Climatic Change* 109: 33-57

847 **Rieder H.E.**, Fiore A.M., Horowitz L.W., Naik V., 2015, “Projecting policy-relevant metrics
848 for high summertime ozone pollution events over the eastern United States due to climate and
849 emission changes during the 21st century”. *J. Geophys. Res. Atmos.* 120: 784-800

850 **Ridley B.A.**, Pickering K.E., Dye, J.E., 2005, “Comments on the parameterization of
851 lightning-produced NO in global chemistry-transport models”. *Atmos. Environ.* 39: 6184-
852 6187

853 **Ochoa-Hueso R.**, Munzi S., Alonso R., Sicard P., Stevens C. et al., 2017, “Ecological
854 Impacts of Atmospheric Pollution and Interactions with Climate Change in Terrestrial
855 Ecosystems of the Mediterranean Basin: Current Research and Future Directions”. *Environ.*
856 *Pollut.* 227: 194-206

857 **Sanderson M.G.**, Collins W.J., Hemming D.L., Betts R.A., 2007, “Stomatal conductance
858 changes due to increasing carbon dioxide levels: Projected impact on surface ozone levels”.
859 *Tellus* 59B: 404-411

860 **Sanderson M.G.**, Jones C.D., Collins W.J., Johnson C.E., Derwent R.G., 2003, “Effect of
861 climate change on isoprene emissions and surface ozone levels”. *Geophys. Res. Lett.* 30: 1936

862 **Schnell J.L.**, Prather M.J., Josse B., Naik V., Horowitz L.W., et al., 2016, “Effect of climate
863 change on surface ozone over North America, Europe, and East Asia”. *Geophys. Res. Lett.* 43:
864 L068060

865 **Seidel D.J.**, Fu Q., Randel W.J., Reichler T.J., 2008, “Widening of the tropical belt in a
866 changing climate”. *Nat. Geosci* 1: 21-4

867 **Shindell D.T.**, Lamarque J.F., Schulz M., Flanner M., Jiao C., et al., 2012, “Radiative forcing
868 in the ACCMIP historical and future climate simulations”. *Atmos. Chem. Phys. Discuss.* 12:
869 21105-21210

870 **Shindell D.T.**, Faluvegi G., Stevenson D.S., Krol M.C., Emmons L.K., et al., 2006, “Multi-
871 model simulations of carbon monoxide: Comparison with observations and projected near-
872 future changes”. *J. Geophys. Res.* 111: D19306

873 **Sicard P.**, Serra R., Rossello P., 2016a, “Spatiotemporal trends of surface ozone
874 concentrations and metrics in France”. *Environ. Res.* 149: 122-144

875 **Sicard P.**, Augustaitis A., Belyazid S., Calfapietra C., De Marco A., et al., 2016b, “Global
876 topics and novel approaches in the study of air pollution, climate change and forest
877 ecosystems”. *Environ. Pollut.* 213: 977-987

878 **Sicard P.**, De Marco A., Dalstein-Richier L., Tagliaferro F., Paoletti E., 2016c, “An
879 epidemiological assessment of stomatal ozone flux-based critical levels for visible ozone
880 injury in Southern European forests”. *Sci. Total Environ.* 541: 729-741

881 **Sicard P.**, De Marco A., Troussier F., Renou C., Vas N., Paoletti E., 2013, “Decrease in
882 surface ozone concentrations at Mediterranean remote sites and increase in the cities”. *Atmos.*
883 *Environ.* 79: 705-715

884 **Sicard P.**, Vas N., Dalstein-Richier L., 2011, “Annual and seasonal trends for ambient ozone
885 concentration and its Impact on Forest Vegetation in Mercantour National Park (South-eastern
886 France) over the 2000-2008 period”. *Environ. Pollut.* 159: 351-362

887 **Sicard P.**, Coddeville P., Galloo J.C., 2009, “Near-surface ozone levels and trends at rural
888 stations in France over the 1995-2003 period”. *Environ. Monit. Assess.* 156: 141-157

889 **Simpson D.**, Arneth A., Mills G., Solberg S., Uddling J., 2014, “Ozone - the persistent
890 menace: interactions with the N cycle and climate change”. *Curr. Opin. Env. Sust.* 9-10: 9-19

891 **Singh H.B.**, Herlth D., O'Hara D., Zahnle K., Bradshaw J.D., et al., 1992, “Relationship of
892 Peroxyacetyl nitrate to active and total odd nitrogen at northern high latitudes: influence of
893 reservoir species on NO_x and O₃”. *J. Geophys. Res.* 97:16523-30

894 **Sitch S.**, Cox P.M., Collins W.J., Huntingford C., 2007, “Indirect radiative forcing of climate
895 change through ozone effects on the land-carbon sink”. *Nature* 448: 791-794

896 **Steinbacher M.**, Henne S., Dommen J., Wiesen P., Prevot A.S.H., 2004, “Nocturnal trans-
897 alpine transport of ozone and its effects on air quality on the Swiss Plateau”. *Atmos. Environ.*
898 38: 4539-4550

899 **Stevenson D.S.**, Young P.J., Naik V., Lamarque J.F., Shindell D.T., et al., 2013,
900 “Tropospheric ozone changes, radiative forcing and attribution to emissions in the
901 Atmospheric Chemistry and Climate Model Inter-comparison Project (ACCMIP)”. *Atmos.*
902 *Chem. Phys.* 13: 3063-3085

903 **Stevenson D.S.**, Young P.J., Naik V., Lamarque J.F., Shindell D.T., et al., 2012,
904 “Tropospheric ozone changes, radiative forcing and attribution to emissions in the
905 Atmospheric Chemistry and Climate Model Inter-comparison Project (ACCMIP)”. *Atmos.*
906 *Chem. Phys. Discuss.* 12: 26047-26097

907 **Stevenson D.S.**, Dentener F.J., Schultz M.G., Ellingsen K., van Noije T.P.C., et al., 2006,
908 “Multi-model ensemble simulations of present-day and near-future tropospheric ozone”. *J.*
909 *Geophys. Res.* 111: D08301

910 **Stevenson D.S.**, Johnson C.E., Collins W.J., Derwent R.G., Edwards J.M., 2000, “Future
911 estimates of tropospheric ozone radiative forcing and methane turnover – The impact of
912 climate change”. *Geophys. Res. Lett.* 27: 2073-2076

913 **Stohl A.**, Berg T., Burkhardt J.F., Fjaeraa A.M., Forster C., et al., 2007, « Arctic smoke -
914 record high air pollution levels in the European Arctic due to agricultural fires in Eastern
915 Europe in spring 2006”. *Atmos. Chem. Phys.* 7: 511-534

916 **Tang Q.**, Prather M.J., Hsu J., 2011, “Stratosphere-troposphere exchange ozone flux related
917 to deep convection”. *Geophys. Res. Lett.* 38: L03806

918 **Teysse re H.**, Michou M., Clark H.L., Josse B., Karcher F., et al., 2007, “A new tropospheric
919 and stratospheric Chemistry and Transport Model MOCAGE-Climat for multi-year studies:
920 evaluation of the present-day climatology and sensitivity to surface processes”. *Atmos. Chem.*
921 *Phys.* 7: 5815-5860

922 **Tian W.**, Chipperfield M., Huang Q., 2008, “Effects of the Tibetan Plateau on total column
923 ozone distribution”. *Tellus* 60B: 622-635

924 **UNECE**, United Nations Economic Commission for Europe. Convention on Long-Range
925 Trans-boundary Air Pollution, 2010, “Mapping Critical Levels for Vegetation”. International
926 Cooperative Programme on Effects of Air Pollution on Natural Vegetation and Crops,
927 Bangor, UK

928 **van Vuuren D.**, Edmonds J., Kainuma M., Riahi K., Thomson A., et al., 2011, “The
929 representative concentration pathways: an overview”. *Climatic Change* 109: 5-31

930 **Voulgarakis A.**, Naik V., Lamarque J.F., Shindell D.T., Young P.J. et al., 2013, “Analysis of
931 present day and future OH and methane lifetime in the ACCMIP simulations”. *Atmos. Chem.*
932 *Phys.* 13: 2563-2587

933 **Walker T.W.**, Jones D.B.A., Parrington M., Henze D.K., Murray L.T., et al., 2012, “Impacts
934 of mid-latitude precursor emissions and local photochemistry on ozone abundances in the
935 Arctic”. *Journal of Geophysical Research: Atmospheres* 117, doi: 10.1029/2011JD016370

936 **Wang Q.Y.**, Gao R.S., Cao J.J., Schwarz J.P., Fahey D.W., et al. 2015, “Observations of high
937 level of ozone at Qinghai Lake basin in the northeastern Qinghai-Tibetan Plateau, western
938 China”. *J. Atm. Chem.* 72: 19-26

939 **Wang X.** and Mauzerall D.L., 2004, “Characterizing distributions of surface ozone and its
940 impact on grain production in China, Japan and South Korea: 1900 and 2020”. *Atmos.*
941 *Environ.* 38: 4383-4402

942 **Watanabe S.**, Hajima T., Sudo K., Nagashima T., Takemura T., et al., 2011, “MIROC-ESM
943 2010: model description and basic results of CMIP5-20c3m experiments”. *Geosci. Model*
944 *Dev.* 4: 845-872

945 **Wesely M.L.** and Hicks B.B., 2000, “A review of the current status of knowledge in dry
946 deposition”. *Atmos. Environ.* 34: 2261-2282

947 **Wild O.**, Fiore A.M., Shindell D.T., Doherty R.M., Collins W.J., et al., 2012, “Modelling
948 future changes in surface ozone: a parameterized approach”. *Atmos. Chem. Phys.* 12: 2037-
949 2054

950 **Wild O.**, 2007, “Modelling the global tropospheric ozone budget: exploring the variability in
951 current models”. *Atmos. Chem. Phys.* 7: 2643-2660

952 **Williams E.R.**, 2009, “The global electrical circuit: A review”. *Atmos. Res.*, 91: 140-152.

953 **Wilson R.C.**, Fleming Z. L., Monks P. S., Clain G., Henne S., et al., 2012, “Have primary
954 emission reduction measures reduced ozone across Europe? An analysis of European rural
955 background ozone trends 1996-2005”. *Atmos. Chem. Phys.* 12: 437-454

956 **Wittig V.E.**, Ainsworth E.A., Naidu S.L., Karnosky D.F., Long S.P., 2009, “Quantifying the
957 impact of current and future tropospheric ozone on tree biomass, growth, physiology and
958 biochemistry: a quantitative meta-analysis”. *Global Change Biol.* 15: 396-424

959 **Wittig V.E.**, Ainsworth E.A., Long S.P., 2007, “To what extent do current and projected
960 increases in surface ozone affect photosynthesis and stomatal conductance of trees? A meta-
961 analytic review of the last 3 decades of experiments”. *Plant, Cell Environ.* 30: 1150-1162

962 **Xing J.**, Mathur R., Pleim J., C. Hogrefe, Gan C.M., et al., 2015, “Observations and modeling
963 of air quality trends over 1990–2010 across the Northern Hemisphere: China, the United
964 States and Europe”. *Atmos. Chem. Phys.* 15: 2723-2747

965 **Young P.J.**, Archibald A.T., Bowman K.W., Lamarque J.F., Naik V., et al., 2013,
966 “Preindustrial to end 21st century projections of tropospheric ozone from the Atmospheric
967 Chemistry and Climate Model Intercomparison Project (ACCMIP)”. *Atmos. Chem. Phys.* 13:
968 2063-2090

969 **Zak D.R.**, Pregitzer K.S., Kubiske M.E., Burton A.J., 2011, “Forest productivity under
970 elevated CO₂ and O₃; positive feedbacks to soil N cycling sustain decade-long net primary
971 productivity enhancement by CO₂. *Ecology Letters* 14: 1220-1226

972 **Zeng G.**, Morgenstern O., Braesicke P., Pyle J.A., 2010, “Impact of stratospheric ozone
973 recovery on tropospheric ozone and its budget”. *Geophys. Res. Lett.* 37: L09805

974 **Zeng G.**, Pyle J.A., Young P. J., 2008, “Impact of climate change on tropospheric ozone and
975 its global budgets, *Atmos. Chem. Phys.* 8: 369-387

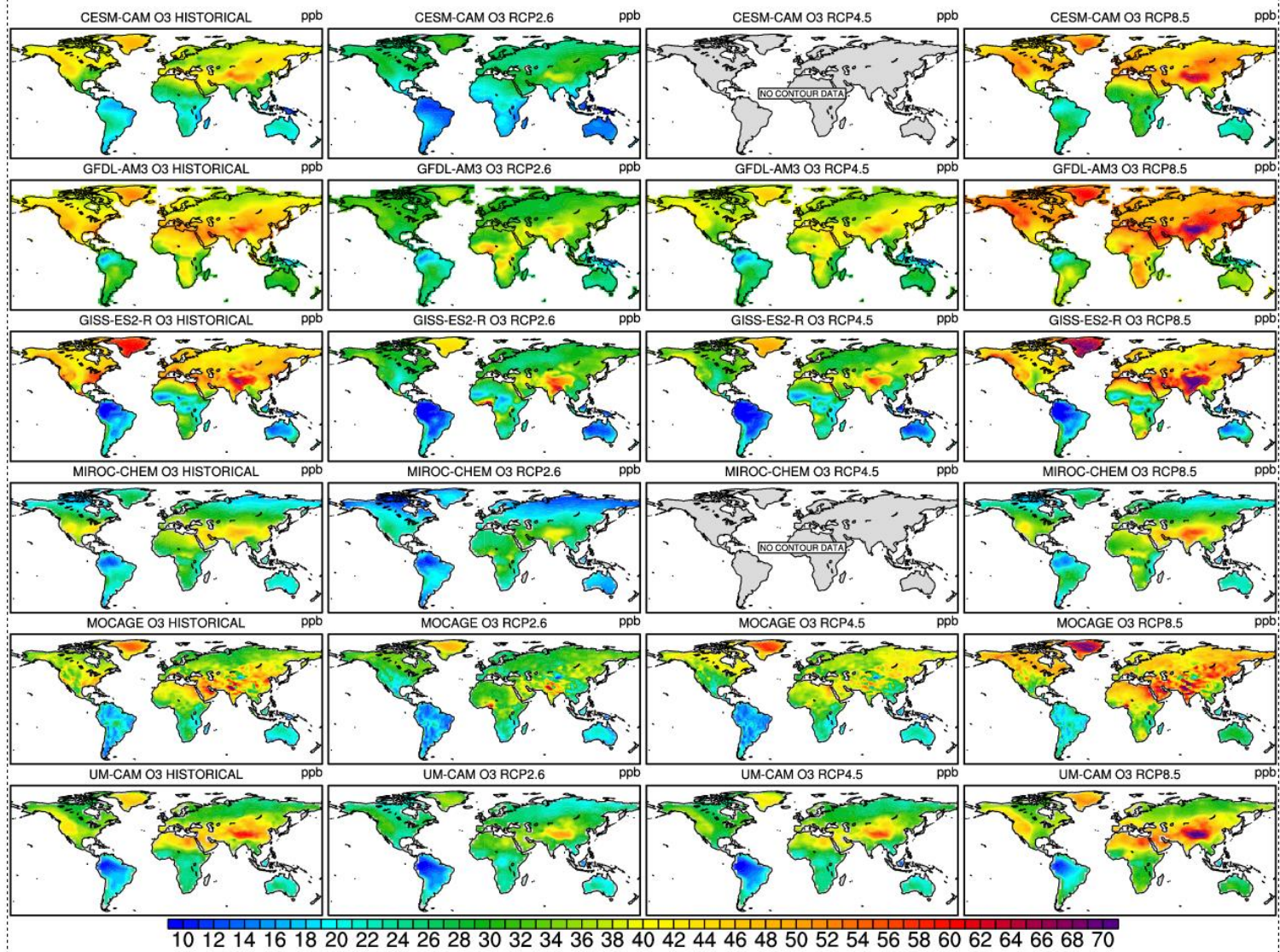
976 **Zeng G.** and Pyle J.A., 2003, “Changes in tropospheric ozone between 2000 and 2100
977 modeled in a chemistry-climate model”. *Geophys. Res. Lett.* 30: 1392

978 **Zhang Q.**, Streets D.G., Carmichael G.R., He K.B., Huo H., et al., 2009, “Asian emissions in
979 2006 for the NASA INTEX-B mission”. *Atmos. Chem. Phys.* 9: 5131-5153

980 **Zhang M.**, Xu Y., Uno I., Akimoto H., 2004, “A numerical study of tropospheric ozone in the
981 springtime in east Asia”. *Adv. Atmos. Sci.* 21: 163-170

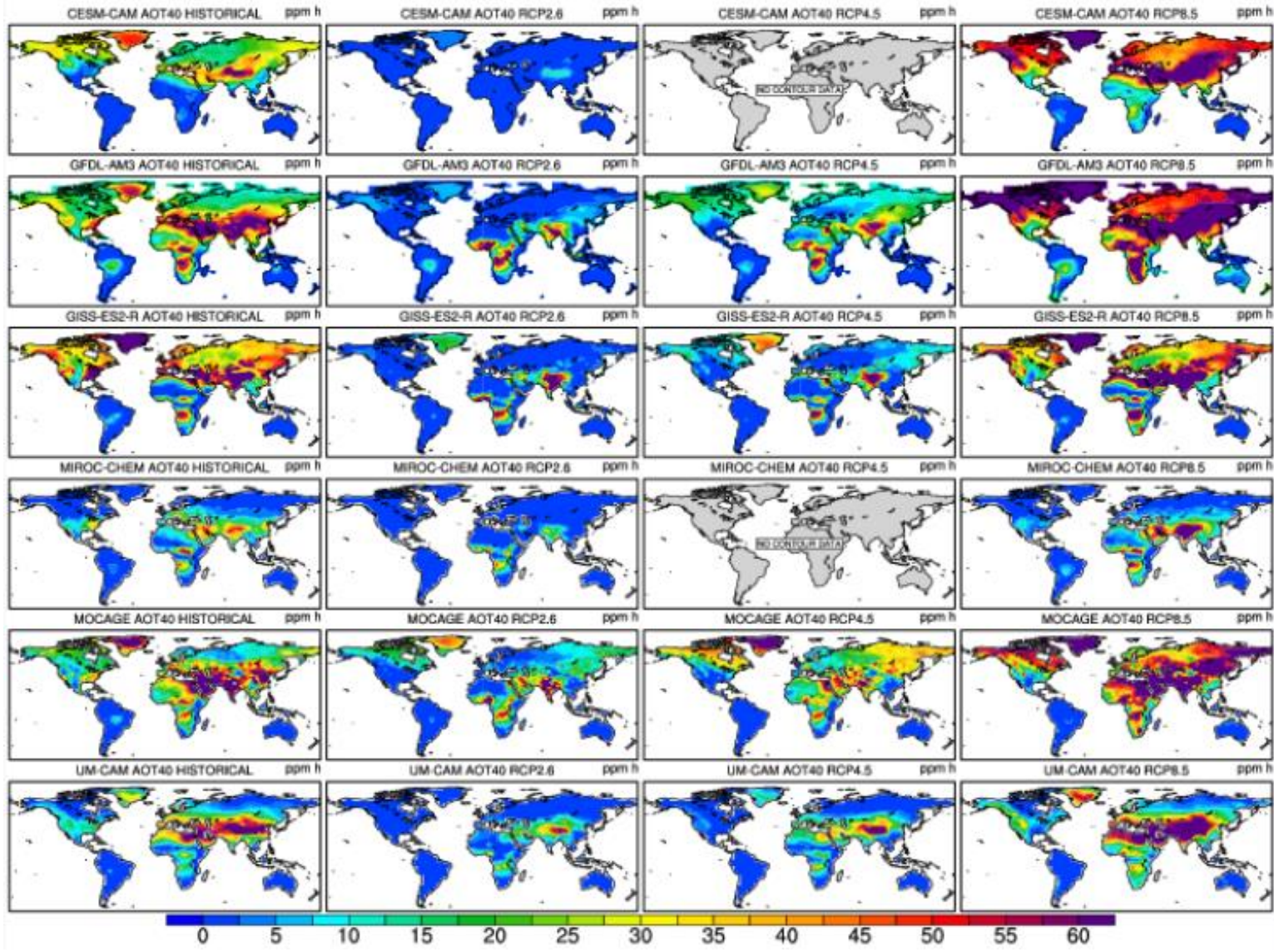
982 **Zhang L.**, Brook J. R., Vet R., 2003, “A revised parameterization for gaseous dry deposition
983 in air-quality models”. *Atmos. Chem. Phys.* 3: 2067-2082
984 **Zhu Z.**, Piao S., Myneni R.B., Huang M., Zeng Z., et al., 2016, “Greening of the Earth and its
985 drivers”. *Nature Climate Change* 6: 791-795
986
987
988
989

990 **Figure 1:** Surface ozone average concentrations (in ppb) at the lower model layer for each ACCMIP model over the historical
991 period and for RCP2.6, RCP4.5 and RCP8.5 simulations by 2100. The data are missing for 2 models under RCP4.5 ("No contour
992 data").



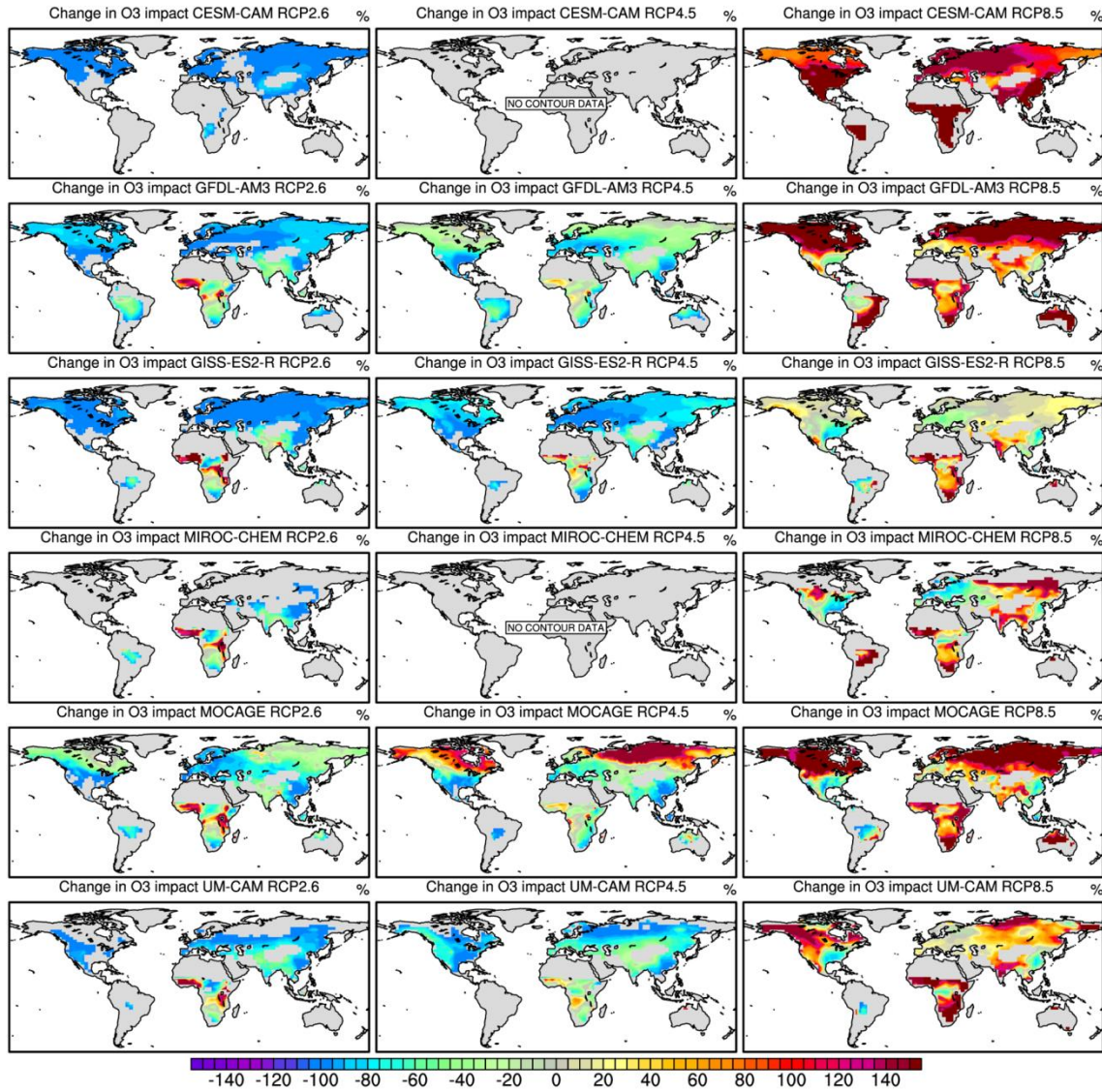
993
994

995 **Figure 2:** Surface mean AOT40 (in ppm.h) at the lower model layer for each ACCMIP model over the historical period and for
 996 RCP2.6, RCP4.5 and RCP8.5 simulations by 2100. The data are missing for 2 models under RCP4.5 ("No contour data").



997

998 **Figure 3:** Simulated percentage changes (%) in the potential ozone impact on photosynthetic carbon assimilation (IO3) for each
999 ACCMIP model between RCP2.6, RCP4.5 and RCP8.5 simulations and the historical run. The data are missing for 2 models under
1000 RCP4.5 ("No contour data").



1002 **Table 1:** Characteristics of the models, including simulation time slice, spatial resolution, simulated gas species and associated
 1003 bibliographic references (from Lamarque et al., 2013 and Young et al. 2013). Black carbon (BC), Organic carbon (OC), Secondary
 1004 Organic Aerosols (SOA), Dimethylsulfide (DMS), Chemistry Climate Model (CCM), Chemistry Transport Model (CTM),
 1005 Chemistry-General Circulation Model (CGCM).
 1006

Models	Type	Simulation length	Resolution (lat/lon)	Number of vertical pressure levels & top level	Species simulated	References
CESM-CAM	CCM	2000-2009 and 2100-2109	1.875/2.5	26 levels 3.5 hPa	16 gas species; constant present-day isoprene, soil NO _x , DMS and volcanic sulfur, oceanic CO.	Lamarque et al., 2012
GFDL-AM3	CCM	2001-2010 and 2101-2110	2.0/2.5	48 levels 0.017 hPa	81 gas species; SO _x , BC, OC, SOA, NH ₃ , NO ₃ ; constant pre-industrial soil NO _x ; constant present-day soil and oceanic CO, and biogenic VOC; climate-sensitive dust, sea salt, and DMS.	Donner et al., 2011 Naik et al., 2012
GISS-E2-R	CCM	2000-2004 and 2101-2105	2.0/2.5	40 levels 0.14 hPa	51 gas species; interactive sulfate, BC, OC, sea salt, dust, NO ₃ , SOA, alkenes; constant present-day soil NO _x ; climate-sensitive dust, sea salt, and DMS; climate-sensitive isoprene based on present-day vegetation.	Lee and Adams, 2011 Shindell et al., 2012
MIROC-CHEM	CCM	2000-2010 and 2100-2104	2.8/2.8	80 levels 0.003 hPa	58 gas species; SO ₄ , BC, OC; constant present-day VOCs, soil-NO _x , oceanic-CO; climate-sensitive dust, sea salt and DMS.	Watanabe et al., 2011
MOCAGE	CTM	2000-2003 and 2100-2103	2.0/2.0	47 levels 6.9 hPa	110 gas species; constant present-day isoprene, other VOCs, oceanic CO and soil NO _x .	Josse et al., 2004 Krinner et al., 2005 Teyssèdre et al., 2007
UM-CAM	CGCM	2000-2005 and 2094-2099	2.50/3.75	19 levels 4.6 hPa	60 gas species; constant present-day biogenic isoprene, soil NO _x , biogenic and oceanic CO.	Zeng et al., 2008, 2010

1007

1008 **Table 2a:** Annual total emissions of CO (Tg CO/year), NMVOCs (Tg C/year), NO_x (Tg N/year, including lightning and soil NO_x),
 1009 total lightning NO_x emissions (LNO_x) and global atmospheric methane (CH₄) burden (Tg) for the historical simulations in each
 1010 model (from Young et al., 2013 and * from Voulgarakis et al., 2013).
 1011

Models	Historical				
	CO	* CH ₄	NMVOCs	NO _x	*LNO _x
CESM-CAM	1248	4902	429	50.0	4.2
GFDL-AM3	1246	4809	830	46.2	4.4
GISS-E2-R	1070	4793	830	48.6	7.7
MIROC-CHEM	1064	4805	833	57.3	9.7
MOCAGE	1168	4678	1059	47.9	5.2
UM-CAM	1148	4879	535	49.2	5.1

1012
 1013
 1014
 1015
 1016
 1017
 1018
 1019
 1020
 1021
 1022 **Table 2b:** Simulated percentage (%) changes in total emissions of CO, NMVOCs, NO_x (including lightning and soil NO_x), total
 1023 lightning NO_x emissions (LNO_x) and global atmospheric CH₄ burden for each model between 2100 and historical simulation for
 1024 RCPs (from Young et al., 2013 and *Voulgarakis et al., 2013). The last row shows means and standard deviations (SD). Missing or
 1025 not available data are identified (n.a).
 1026

Models	RCP2.6 scenario					RCP4.5 scenario					RCP8.5 scenario				
	CO	VOCs	NO _x	*LNO _x	*CH ₄	CO	VOCs	NO _x	*LNO _x	*CH ₄	CO	VOCs	NO _x	*LNO _x	*CH ₄
CESM-CAM	- 36.7	0	- 52.8	+ 7.1	- 27.1	n.a	n.a	n.a	n.a	n.a	- 30.1	0	- 33.0	+ 29.7	+ 112.1
GFDL-AM3	- 36.9	- 5.0	- 47.0	+ 12.6	- 27.9	- 47.4	- 3.6	- 41.5	+ 23.5	- 9.3	- 30.3	- 1.9	- 22.4	+ 38.2	+ 116.1
GISS-E2-R	- 42.8	+ 0.5	- 44.2	+ 3.8	- 21.0	- 54.9	+ 6.9	- 39.2	+ 12.2	+ 4.6	- 35.1	+ 19.8	- 20.0	+ 26.2	+ 152.7
MIROC-CHEM	- 43.1	- 7.1	- 36.0	+ 7.5	- 28.2	n.a	n.a	n.a	n.a	n.a	- 35.4	- 3.4	- 6.9	+ 38.0	+ 116.0
MOCAGE	- 39.4	- 6.5	- 45.7	+ 5.2	- 28.8	n.a	n.a	n.a	n.a	n.a	- 32.3	- 2.8	- 22.9	+ 19.9	+ 113.4
UM-CAM	- 39.0	- 11.3	- 40.6	+ 8.1	- 27.9	- 50.4	- 9.2	- 36.0	+ 17.5	- 8.7	- 32.0	- 4.2	- 17.2	+ 43.6	+ 112.1
Mean ± SD	- 39.7 ± 2.2	- 4.9 ± 4.9	- 44.4 ± 4.3	+ 7.4 ± 2.0	- 26.8 ± 3.7	- 50.9 ± 3.2	- 2.0 ± 11.4	- 38.9 ± 2.3	+ 17.7 ± 3.7	- 4.5 ± 9.4	- 32.5 ± 1.8	+ 1.3 ± 11.6	- 20.4 ± 7.0	+ 32.6 ± 10.8	+ 120.4 ± 19.5

1027
 1028

1029 **Table 3a:** Global and hemispheric (averaged over the domain) mean annual-average surface ozone concentrations (in ppb) and
 1030 mean AOT40 (in ppm.h) for the historical simulations in each model (North and South Hemisphere, i.e NH and SH). The last row
 1031 shows means and standard deviations (SD).
 1032

Models	Ozone conc. global	Ozone conc. SH	Ozone conc. NH	AOT40 global	AOT40 SH	AOT40 NH
CESM-CAM	31.3	20.9	36.4	12.8	0.2	18.9
GFDL-AM3	38.6	30.6	42.9	21.8	4.7	30.8
GISS-E2-R	35.8	22.3	42.3	26.0	3.6	36.8
MIROC-CHEM	27.9	20.4	31.4	7.3	1.9	9.8
MOCAGE	32.9	21.5	38.3	22.9	3.5	31.8
UM-CAM	31.3	21.4	36.0	14.4	1.3	20.6
Mean \pm SD	33.0 \pm 3.8	22.9 \pm 3.8	37.9 \pm 4.3	17.5 \pm 7.2	2.5 \pm 1.7	24.8 \pm 10.1

1033
 1034
 1035
 1036
 1037
 1038
 1039
 1040

Table 3b: Simulated percentage (%) changes in global and hemispheric mean annual-average surface ozone concentrations and in
 global mean stratospheric ozone column (* from Voulgarakis et al., 2013) for each model between 2100 and historical simulation
 for RCPs (North and South Hemisphere, i.e NH and SH). The last row shows means and standard deviations (SD). Missing or not
 available data are identified (n.a).

Models	Surface ozone mean concentrations									* Stratospheric ozone		
	RCP2.6 global	RCP2.6 SH	RCP2.6 NH	RCP4.5 global	RCP4.5 SH	RCP4.5 NH	RCP8.5 global	RCP8.5 SH	RCP8.5 NH	RCP2.6 global	RCP4.5 global	RCP8.5 global
CESM-CAM	- 29.1	- 20.6	- 31.3	n.a	n.a	n.a	+ 21.9	+ 22.5	+ 20.5	n.a	n.a	+ 5.3
GFDL-AM3	- 20.5	- 10.8	- 24.5	- 11.7	- 6.9	- 13.5	+ 15.5	+ 18.6	+ 14.5	+ 3.3	+ 3.9	+ 8.4
GISS-E2-R	- 23.5	- 5.8	- 27.9	- 20.4	- 6.3	- 23.9	+ 7.0	+ 19.3	+ 3.8	+ 8.0	+ 8.8	+ 15.1
MIROC-CHEM	- 23.3	- 12.3	- 26.8	n.a	n.a	n.a	+ 3.9	+ 10.3	+ 2.2	+ 2.6	n.a	+ 4.2
MOCAGE	- 12.8	+ 7.4	- 18.5	- 1.8	+ 17.7	- 7.0	+ 23.1	+ 40.4	+ 16.7	+ 19.9	n.a	+ 23.6
UM-CAM	- 17.3	- 4.7	- 21.1	- 8.3	+ 0.9	- 10.8	+ 14.4	+ 24.3	+ 11.4	+ 6.7	+ 6.9	+ 7.4
Mean \pm SD	- 21.1 \pm 5.6	- 7.8 \pm 9.4	- 25.0 \pm 4.7	- 10.5 \pm 7.7	+ 1.4 \pm 11.5	- 13.8 \pm 7.2	+ 13.8 \pm 7.1	+ 22.6 \pm 10.0	+ 11.5 \pm 7.3	+ 8.1 \pm 7.0	+ 6.5 \pm 2.5	+ 10.7 \pm 7.4

1041
 1042

1043 **Table 3c:** Simulated percentage (%) changes in global and hemispheric mean AOT40 for each model between 2100 and historical
 1044 simulation for RCPs (North and South Hemisphere, i.e NH and SH). Missing or not available data are identified (n.a).
 1045

Models	AOT40								
	RCP2.6 global	RCP2.6 SH	RCP2.6 NH	RCP4.5 global	RCP4.5 SH	RCP4.5 NH	RCP8.5 global	RCP8.5 SH	RCP8.5 NH
CESM-CAM	- 96.9	- 99.9	- 96.8	n.a	n.a	n.a	+ 138.3	+ 150.0	+ 134.9
GFDL-AM3	- 75.2	- 25.5	- 78.9	- 53.2	- 36.2	- 54.5	+ 96.3	+ 242.5	+ 85.1
GISS-E2-R	- 78.1	- 13.9	- 81.2	- 75.0	- 27.8	- 77.2	+ 22.3	+ 83.3	+ 19.5
MIROC-CHEM	- 74.0	- 10.5	- 80.6	n.a	n.a	n.a	+ 20.5	+ 78.9	+ 16.3
MOCAGE	- 53.7	+ 68.6	- 59.7	- 17.5	+ 202.9	- 28.3	+ 85.1	+ 448.6	+ 67.0
UM-CAM	- 73.6	+ 92.3	- 76.7	- 52.8	+ 7.7	- 54.8	+ 49.3	+ 176.9	+ 45.1
Mean ± SD	- 75.2 ± 13.7	+ 1.9 ± 69.5	- 79.0 ± 11.8	- 49.6 ± 23.8	+ 36.6 ± 112.4	- 53.7 ± 20.0	+ 68.6 ± 46.3	+ 196.7 ± 137.7	+ 61.3 ± 44.8

1046
 1047
 1048 **Table 3d:** Simulated percentage (%) changes in potential O₃ impact on vegetation (IO3) for each model between 2100 and historical
 1049 simulation for RCPs (North and South Hemisphere, i.e NH and SH).Missing or not available data are identified (n.a).
 1050

Models	Risk factor IO3								
	RCP2.6 global	RCP2.6 SH	RCP2.6 NH	RCP4.5 global	RCP4.5 SH	RCP4.5 NH	RCP8.5 global	RCP8.5 SH	RCP8.5 NH
CESM-CAM	- 97.2	- 91.8	-97.5	n.a	n.a	n.a	+ 129.6	+146.8	+127.5
GFDL-AM3	- 69.4	- 49.1	- 74.8	- 50.1	- 61.1	- 47.2	+ 91.9	+95.5	+90.4
GISS-E2-R	- 66.1	- 20.7	- 74.3	- 71.7	- 53.3	- 74.6	+ 21.5	+56.6	+14.2
MIROC-CHEM	- 41.4	- 18.9	- 51.9	n.a	n.a	n.a	+ 41.0	+103.8	+25.5
MOCAGE	- 46.6	-22.8	- 51.4	- 7.0	- 38.0	- 1.0	+ 77.7	+68.2	+80.0
UM-CAM	- 45.8	- 9.2	- 71.3	- 59.5	+ 2.0	- 69.0	+ 61.3	+84.2	+56.0
Mean ± SD	- 61.1 ± 21.1	- 35.5 ± 30.7	- 70.2 ± 17.2	- 47.1 ± 28.1	- 37.6 ± 28.1	- 47.9 ± 33.4	+ 70.5 ± 38.4	+ 92.5 ± 31.7	+ 65.6 ± 42.4

1051